

ANALYSIS OF WOUND IRRIGATION DEVICES

by

Amogh Madan Pawar

A thesis submitted to the faculty of
The University of North Carolina at Charlotte
in partial fulfillment of the requirements
for the degree of Master of Science in
Mechanical Engineering

Charlotte

2018

Approved by:

Dr. Tony Schmitz

Dr. Charles Lee

Dr. Naiquan Zheng

©2018
Amogh Madan Pawar
ALL RIGHTS RESERVED

ABSTRACT

AMOGH MADAN PAWAR. Analysis of wound irrigation devices. (Under the direction of DR. TONY SCHMITZ)

In wound irrigation, the surface pressure at the wound is critical. Correct pressure ensures removal of bacteria and foreign debris without further tissue damage. Surface pressure measurements were performed for three irrigation devices, including a 500-ml bottle with four holes in the pouring cap, a 60 ml Syringe Monoject™ COVIDIEN™ syringe, and a Sterile IRIG-8™ Wound Irrigation System from CENTURION™. A setup was designed to perform the measurements and subsequent data analysis. This setup included a 3D printed target, containers to catch the fluid, a force dynamometer, and a camera to capture the stream image. Doctors and nurses performed irrigation trials using the three devices. The pressure at the target area was calculated by dividing the time-dependent force by the cross-sectional area of the irrigation fluid stream/streams. An uncertainty analysis was completed to evaluate the measured pressure uncertainty. Mean, minimum, and maximum pressure values were calculated for each trial. The time to complete each trial was also recorded. A method for measuring the surface pressure in wound irrigation using various irrigation devices was realized.

ACKNOWLEDGEMENTS

Foremost, I would like to express my gratitude to Dr. Tony Schmitz for giving me an opportunity to conduct research and for his continuous support and encouragement throughout. I would also like to thank Dr. Charles Lee and Dr. Naiquan Zheng for agreeing to serve on my thesis committee. I am grateful to Dr. Elias Awad for his hospitality during my visit to the Carolina Medical Center and for the help provided to complete this research. I would like to thank my fellow students Prithiviraj Shanmugam and Ryan Copenhaver for ideas and suggestions. Also, this research would not have been possible without Dr. Jeffrey Raquet's aid in 3D printing. I would like to extend my gratitude to the Mechanical Engineering and Engineering Science department for providing me with the necessary facilities and resources for the completion of this research. Lastly, I would like to thank the Graduate School at the University of North Carolina at Charlotte for providing a graduate assistantship during the duration of the research.

DEDICATION

To my parents for their support, guidance and constant encouragement.

TABLE OF CONTENTS

LIST OF TABLES	ix
LIST OF FIGURES	x
1. INTRODUCTION	1
2. METHODOLOGY	4
2.1 Participants	4
2.2 Settings	4
2.3 Irrigation devices	4
2.3.1 500 ml bottle with the four holes in the pouring cap	4
2.3.2 60 ml Syringe Monoject™ COVIDIEN™	5
2.3.3 Sterile IRIG-8™ Wound Irrigation System CENTURION™	5
2.4 Method	6
2.5 Experimental setup	7
2.5.1 3D printed setup	7
2.5.2 Dynamometer	9
2.5.3 Amplifier	10
2.5.4 DAQ	10
2.5.5 Acquisition software	11
2.5.6 DSLR camera	12
2.6 Procedure	12

3. FORCE DATA ANALYSIS	17
3.1 High frequency noise	17
3.2 Filter selection	18
3.2.1 Normalized cut off frequency	19
3.2.2 Order of the Butterworth filter	21
3.2.3 Drift compensation and DC offset removal	23
3.3 Resultant force calculation for all 60 trials	26
4. STREAM AREA ANALYSIS	28
4.1 Selection of an edge detection tool	28
4.2 Preprocessing before canny edge detection	28
4.3 Canny edge detection	30
4.4 Stream impact area calculation	34
4.4.1 Impact fluid area for bottle with four holes in the pouring cap (irrigation device 1)	34
4.4.2 Impact fluid area with syringe (irrigation device 2)	35
4.4.3 Impact fluid area with pressurized irrigation device (irrigation device 3)..	35
5. PRESSURE CALCULATION	37
6. UNCERTAINTY ANALYSIS	39
6.1 Propagation of uncertainty	39
6.1.1 500 ml bottle with four holes in pouring cap (irrigation device 1).....	39

6.1.2	60 ml syringe (irrigation device 2).....	40
6.1.3	Pressurized irrigation device (irrigation device 3).....	40
6.2	Combined standard uncertainty.....	41
6.2.1	Calculation of mean values of independent quantities	42
6.2.2	Sensitivity coefficients (c_i).....	46
6.2.3	Standard uncertainty (u_i).....	47
6.3	Expanded uncertainty.....	49
7.	RESULTS AND DISCUSSION.....	56
7.1	Pressure obtained at wound area (target area).....	56
7.1.1	Mean pressure obtained in each trial	56
7.1.2	Mean of mean pressures for each irrigation device	58
7.1.3	Minimum, maximum, and mean pressures calculated for all trials	59
7.2	Force obtained at wound area (target area)	61
7.2.1	Mean force obtained in each trial.....	61
7.2.2	Mean of mean force for each irrigation device.....	62
7.3	Time taken for fluid irrigation.....	63
7.3.1	Duration of each trial	63
7.3.2	Standard deviation of duration of each trial.....	64
8.	CONCLUSION	65
	REFERENCES	67

LIST OF TABLES

Table 6-1 Mean values of independent variables	45
Table 6-2: Combined uncertainty and expanded uncertainty values using bottle with four holes in pouring cap for first 10 participants	50
Table 6-3: Combined uncertainty and expanded uncertainty values using bottle with four holes in pouring cap next 10 participants	51
Table 6-4: Combined uncertainty and expanded uncertainty values using syringe for first 10 participants.....	52
Table 6-5: Combined uncertainty and expanded uncertainty values using syringe for next 10 participants.....	53
Table 6-6: Combined uncertainty and expanded uncertainty values using pressurized device for first 10 participants	54
Table 6-7: Combined uncertainty and expanded uncertainty values using pressurized device for next 10 participants.....	55
Table 7-1: Mean pressure for all participants with expanded uncertainty estimation	57

LIST OF FIGURES

Figure 2-1 Irrigation device no.1: Bottle with four holes in pouring cap	5
Figure 2-2 Irrigation device no. 2: 60 ml Syringe Monoject™ COVIDIEN™	5
Figure 2-3 Irrigation device no. 3: Sterile IRIG-8™ Wound Irrigation System CENTURION™	6
Figure 2-4 3D PTC Creo 3.0 model of the measurement setup.....	7
Figure 2-5 3D printed measurement setup (target area and containers)	9
Figure 2-6 Kistler 9256C1 dynamometer [15].....	10
Figure 2-7 Kistler 5814B1 dual mode amplifier.....	10
Figure 2-8 DT9837B DAQ module	11
Figure 2-9 SPINSCOPE.....	11
Figure 2-10 Canon EOS Digital SLR camera [19]	12
Figure 2-11 3D printed parts and dynamometer setup.....	13
Figure 2-12 Procedure Flowchart	13
Figure 2-13 Experimental setup (full setup)	16
Figure 2-14 Experimental setup (individual views).....	16
Figure 3-1 Raw force data in the time domain	17
Figure 3-2 Raw force data in the frequency domain.....	19
Figure 3-3 Raw force data for no load condition in the frequency domain	20
Figure 3-4 Filtered force data measurements with filter order one to five	22

Figure 3-5 Filtered force data (F_z) in the time domain.....	23
Figure 3-6 Filtered and truncated force data (F_z)	24
Figure 3-7 Final filtered force data with slope and offset removal.....	26
Figure 3-8 Final resultant force data (F)	27
Figure 4-1 Irrigation device images taken by a DSLR camera during fluid impact: (a) bottle with four holes in pouring cap; (b) syringe; (c) pressurized device.	29
Figure 4-2 (a) before edge detection for participant 13 using the bottle with four holes in pouring cap; (b) after edge detection for participant 13 using the bottle with four holes in pouring cap.....	32
Figure 4-3 (a) before edge detection for participant 13 using the syringe; (b) after edge detection for participant 13 using the syringe.....	32
Figure 4-4 (a) before edge detection for participant 13 using the pressurized device; (b) after edge detection for participant 13 using the pressurized device	33
Figure 4-5 (a) before edge detection of the post for participant 13; (b) after edge detection of the post for participant 13.....	33
Figure 5-1 Pressure vs. time for participant 13 using the three irrigation devices	37
Figure 6-1 Bottle with four holes in pouring cap.....	43
Figure 6-2 Syringe	43
Figure 6-3 Pressurized device.....	43
Figure 7-1 Mean pressure for all participants with expanded uncertainty associated with each trial.....	56
Figure 7-2 Mean pressure of all participants with mean expanded uncertainty for the three irrigation devices.....	58

Figure 7-3 Standard deviation of mean pressures for each irrigation device	59
Figure 7-4 Mean, maximum, and minimum pressures for all participants using the bottle with four holes in the pouring cap	60
Figure 7-5 Mean, maximum, and minimum pressures for all participants using the 60 ml syringe.....	60
Figure 7-6 Mean, maximum, and minimum pressures for all participants using the pressurized device	61
Figure 7-7 Mean force for all trials using the three irrigation devices	61
Figure 7-8 Mean force for all trials using the three irrigation devices	62
Figure 7-9 Duration of each trial for all participants using the three irrigation devices...	63
Figure 7-10 Standard deviation of mean trial duration of all participants	64

1. INTRODUCTION

Each year there are millions of emergency department visits for wound treatment in the United States [1]. Proper wound management is essential to prevent infection and ensure better and faster healing [2]. Rapid healing is best accomplished by providing an optimized environment [3]. Wound irrigation is one of the most important features of wound management [4] and is widely accepted as one of the best methods for wound cleansing [5].

Wound irrigation is defined as the steady flow of a fluid across an open wound for removal of bacteria, necrotic tissue, and deeper debris [6]. It also helps in visual inspection of the wound by identifying source of bleeding and determining if there is an emergency surgical concern [2]. There are different methods of irrigating a wound. Traditionally, devices such as bulb syringes, syringes with an attached needle, and a plastic container with a cap or nozzle have been used to deliver the irrigation fluid to the wound. The medical devices presently used are designed to provide a steadier wound pressure [2]. The three key factors that influence the efficiency of wound irrigation are irrigation pressure, volume, and solution. Of these, the irrigation solution is less important than the other two [7]. According to Mitra *et al.* [8], irrigation pressure is the most important wound irrigation factor. Surface pressure lower than the ideal will not be sufficient for bacterial removal. Also, pressure higher than the ideal can cause tissue damage and increase the potential for further contamination [8].

High pressure irrigation has been widely described as an important aspect of effective wound irrigation. However, the required pressure has not been standardized within the medical community. According to Wedmore *et al.* [9], irrigation pressure between 15 and

25 psi constitutes as high-pressure irrigation. In another study, high pressure irrigation was defined from 5 to 8 psi [10]. Singer *et al.* [3] identified pressure greater than 7 psi as high-pressure irrigation. Determining the actual wound surface pressure is required to standardize 'high pressure' irrigation.

A research study completed by Nicks *et al.* [2] points out a lack of substantial literature regarding the deliverable irrigation pressure, with many studies failing to measure the actual pressure. Nicks *et al.* [2] also note that many studies failed to describe the method used for measurement of the wound pressure. Studies that do describe a method of measurement have done so using different models for the irrigation pressure measurement. A standard method with evaluation of the measurement uncertainty is required to improve understanding of irrigation pressure.

Classically, Bernoulli's equation was used to measure the impact pressure at the wound area. A study by Mitra *et al.* [8] showed that the values obtained from Bernoulli's equation differ from the actual wound surface impact pressure and, therefore, it does not offer an effective wound pressure measurement. This is due to assumptions including steady, incompressible, one dimensional, and laminar flow. Mitra *et al.* [8] measured the pressure by directing the stream from the irrigation device on a metal beam. Bending of the beam deflected a laser onto a calibrated wall scale. However, Mitra *et al.* [8] did not measure the actual impact area, but rather assumed that the cross-sectional area of the impact stream was equal to the cross-sectional area of the respective exit lumen. Another limitation of this study was that it took place in a controlled environment and, therefore, did not represent a clinical setting. Also, pressure measurement was a secondary purpose in this study.

In a study by Singer *et al.* [4] two inline Transpac® IV Disposable pressure transducers were used along with other setup for measuring wound pressure using various irrigation devices. However, as noted by Singer *et al.* [4], since measurement in an open system is complex the pressure transducers measured pressure in a closed system. Hence, the actual surface wound pressure was not measured in these trials.

Here, surface wound pressure was calculated from measurements of: 1) the fluid stream force at the point of impact; and 2) the cross-sectional area of the fluid at the same location. The force was measured by a piezoelectric force sensor; force data filtering was implemented in MATLAB® R2017a. The stream's cross-sectional area was calculated by using canny edge detection in MATLAB® R2017a. to locate the fluid stream edges and, therefore, the fluid stream diameter. An uncertainty analysis was performed to evaluate the pressure measurement uncertainty. Based on the literature survey, this pressure measurement has not been previously implemented and offers a first step in standardizing wound surface pressure measurement in clinical environments. The pressure calculation was completed for 20 participants using three different irrigation devices: a 500-ml bottle with four holes in the pouring cap, a 60 ml Syringe Monoject™ COVIDIEN™ syringe, and a Sterile IRIG-8™ Wound Irrigation System from CENTURION™. The duration of each of the 60 trials was also recorded.

2. METHODOLOGY

2.1 Participants

There was a total of 20 participants. The participants consisted of medical students, interns, upper level residents, attending physicians, and nurse practitioners. Each participant used three irrigation devices to perform the tests. Therefore, a total of 60 trials were conducted in this research.

2.2 Settings

The experimental trials were conducted at Carolina Medical Center Emergency Department in Charlotte, NC. They were conducted on June 12th and 13th, 2017.

2.3 Irrigation devices

Sterile water was used as the irrigation fluid. The fluid volume was 500 ml. The three irrigation devices are shown in Figures 2.1-2.3. They are described in the following paragraphs.

2.3.1 500 ml bottle with the four holes in the pouring cap

As the bottle is inverted and manually compressed, the irrigation fluid in the bottle flows out through the four holes in the pouring cap and onto the wound surface to be irrigated; see Figure 2.1.

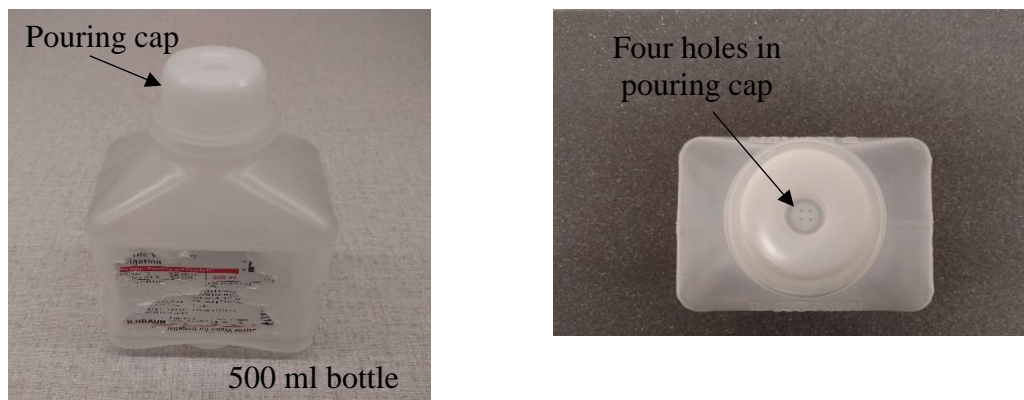


Figure 2-1 Irrigation device no.1: Bottle with four holes in pouring cap

2.3.2 60 ml Syringe Monoject™ COVIDIEN™

After the syringe is filled, the plunger is manually depressed to release the irrigation fluid through the opening onto the wound surface; see Figure 2.2. The 60 ml syringe was refilled multiple times to apply the 500 ml total volume of irrigation fluid.

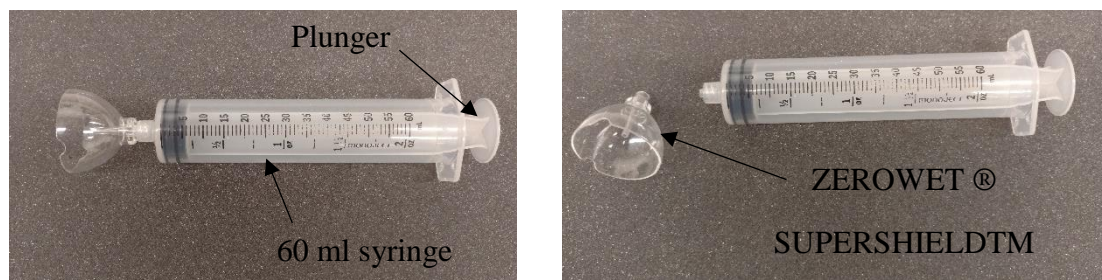


Figure 2-2 Irrigation device no. 2: 60 ml Syringe Monoject™ COVIDIEN™

2.3.3 Sterile IRIG-8™ Wound Irrigation System CENTURION™

This wound irrigation system uses oxygen or compressed air to apply the fluid. Oxygen was used in these trials with an oxygen flowmeter adapter controlling the liters per min flow rate setting. A flow rate of 2.5 liters per minute was set for these trials. The cap was attached to a 600 ml bottle.

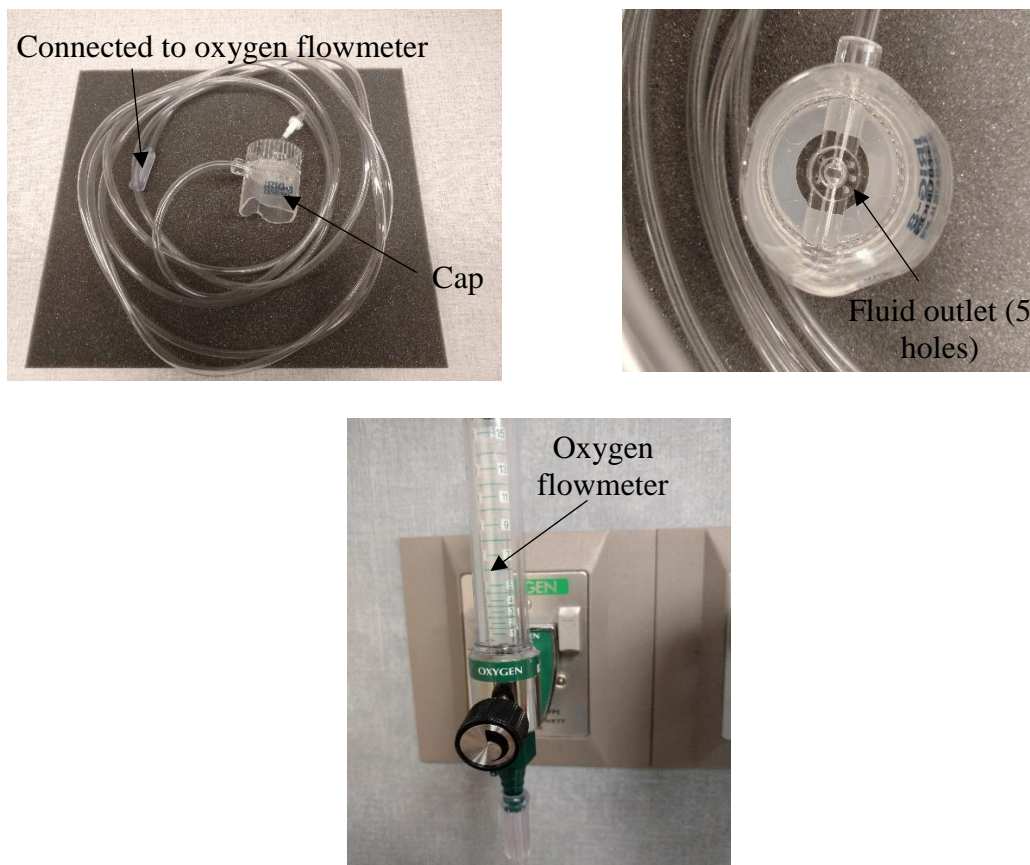


Figure 2-3 Irrigation device no. 3: Sterile IRIG-8™ Wound Irrigation System CENTURION™

2.4 Method

Measurement of pressure at the wound due to the irrigation devices was done by measuring the impact force at the target area and dividing it by the cross-sectional area of the irrigation fluid near the point of impact (shown in equation 2.1). The impact force was measured by a force sensor, while the impact area was found by using image processing tools in MATLAB® R2017a.

$$P = \frac{F}{A} \quad (2.1)$$

where,

P = Pressure at the wound surface (target area)

F = Force near the fluid stream point of impact

A = Cross sectional area of the fluid stream

2.5 Experimental setup

2.5.1 3D printed setup

The 3D modeling software PTC Creo 3.0 (Parametric Technologies Corp., Needham, MA, USA) was used to model the setup. The setup to be 3D printed consisted of a cylindrical post with a larger radius cylindrical top and two containers; see Figure 2.4. The circular surface of the cylindrical top (target area) is a representation of the wound area, while the purpose of the containers is to collect the runoff water during the irrigation trials.

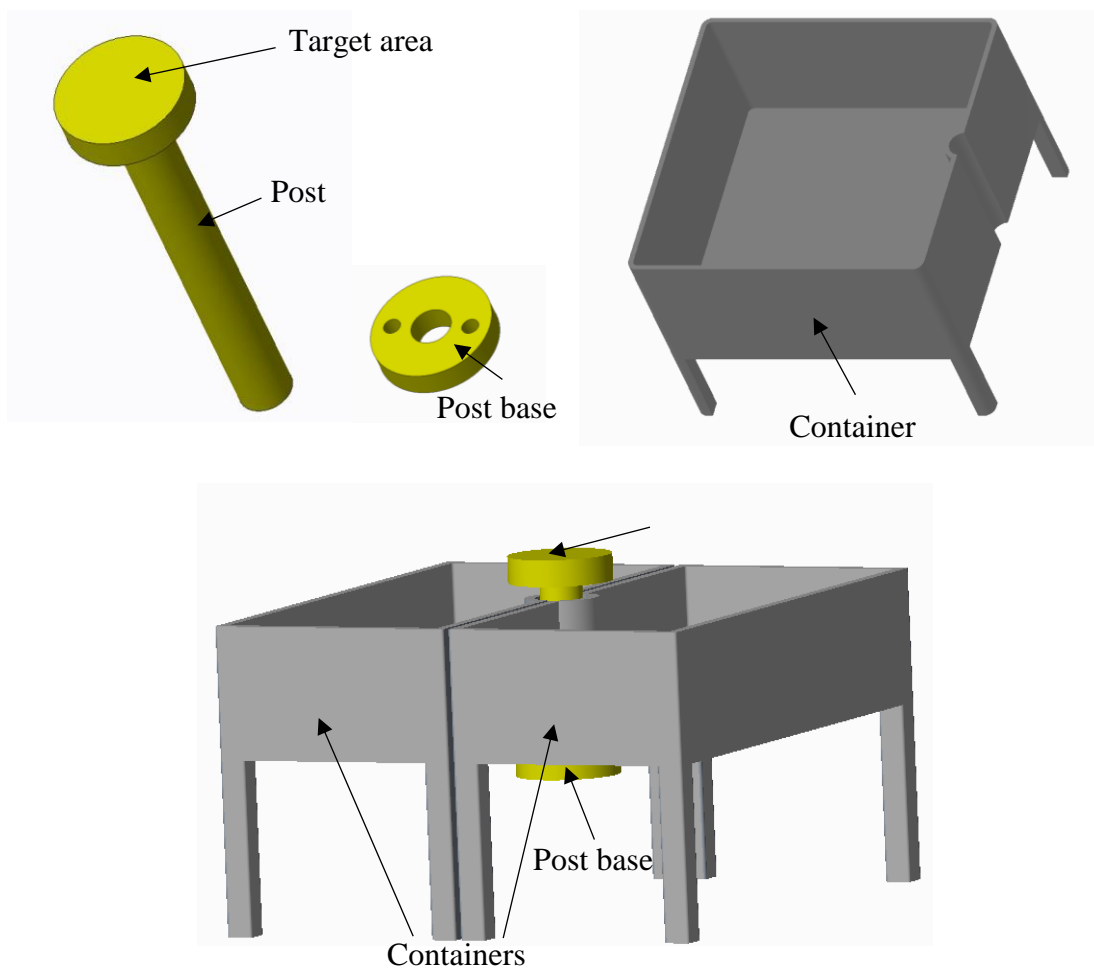


Figure 2-4 3D PTC Creo 3.0 model of the measurement setup

Formlabs' Form 2 3D printer was used to print the two containers shown in Figure 2.4. This printer uses stereolithography. The models designed in PTC Creo needed to be converted into a 'language' that the 3D printer can understand. Standard Tessellation Language (STL) is a language that is mostly used in the stereolithography method of printing. Converting to a STL file slices the CAD data into thin layers. Therefore, after saving the PTC Creo files in the STL format, they were transferred into the SLA system to be printed. Stereolithography is a printing method which uses a UV laser beam to convert liquid resins to a solid [11]. Formlabs' Grey FLGPGR02 was used as the resin material for 3D printing the two containers.

The post and the post base (shown in Figure 2.1) were printed on a Fortus 360mc which uses Fused Deposition Modeling (FDM). The PTC Creo models were saved as an STL data file and then transferred to a slicer software which translated the STL file into a g-code file for 3D printing. Then the files were sent to the FDM 3D printer to be printed. In an FDM system, the modeling material and the filler material are unwound from a coil and passed through a heated extrusion nozzle while in the form of plastic threads. This is done as soon as the nozzle reaches the desired temperature. The filaments are melted by the heated nozzle and then extruded onto the base, layer by layer in a predetermined path. After being extruded, each thin plastic layer cools down and solidifies, therefore binding itself to the layer beneath it [12]. ABS-M30 was the modeling material used for printing the post and the post base.

After the 3D printing process was done, the post and the post base were glued together using epoxy. The 3D printed parts are shown in Figure 2.5.

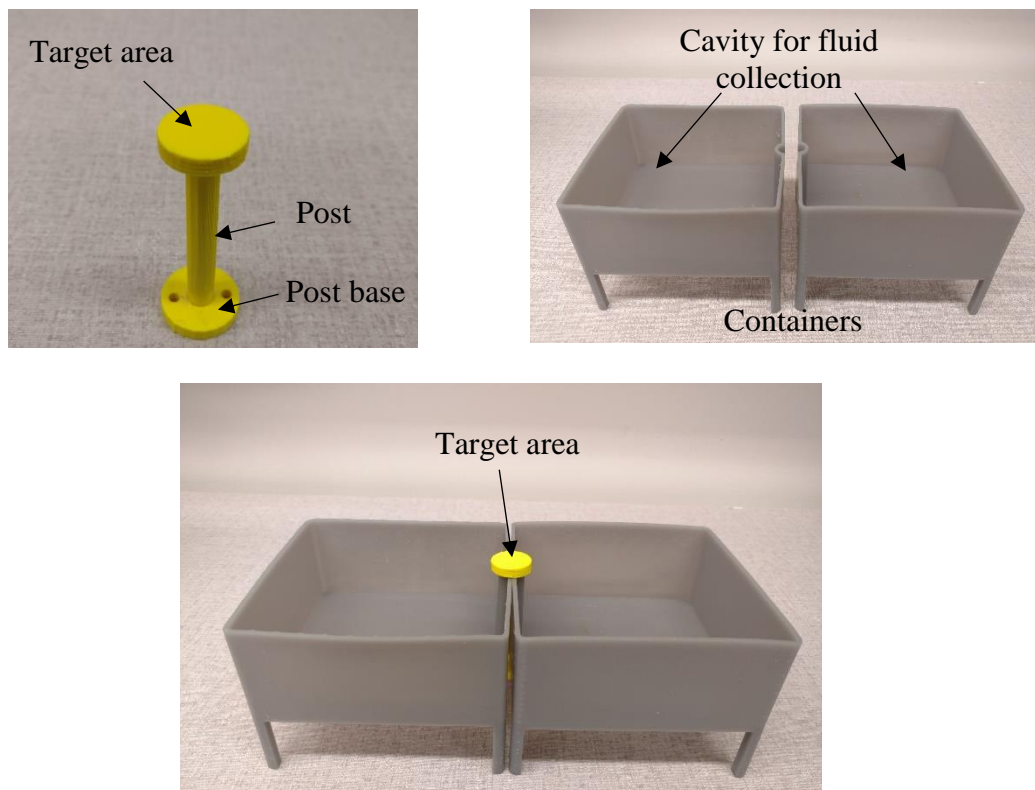


Figure 2-5 3D printed measurement setup (target area and containers)

2.5.2 Dynamometer

A sensor is a device which converts a physical parameter into a measurable electrical signal [13]. A Kistler 9256C1 dynamometer is a force sensor (shown in Figure 2.6) used for the conversion of forces into a voltage output. It is a piezoelectric dynamometer with high sensitivity, high natural frequency and small temperature error [14].



Figure 2-6 Kistler 9256C1 dynamometer [15]

2.5.3 Amplifier

Signal amplification is a type of signal processing where the weak analog signal from the transducer is amplified. A Kistler 5814B1 Dual mode amplifier (see Figure 2.7) was used for the signal amplification and conversion of charge signal from the dynamometer into a proportional output voltage [16].



Figure 2-7 Kistler 5814B1 dual mode amplifier

2.5.4 DAQ

A data acquisition system acts as an interface between the transducer and the computer [16]. DT9837B is a multifunction data acquisition module for the USB bus with four 24-bit sigma-delta ADC converters. It samples the input analog signal at

46.875kSamples/s, converting it into a digital signal [17]. The device drivers needed were stored in a pen drive which was connected to the computer through a USB port.



Figure 2-8 DT9837B DAQ module

2.5.5 Acquisition software

An acquisition software is used to record and store the digital output from the DAQ module. SPINSCOPE, (see Figure 2.9) a virtual oscilloscope product from Manufacturing Laboratories Inc. was used in these trials.

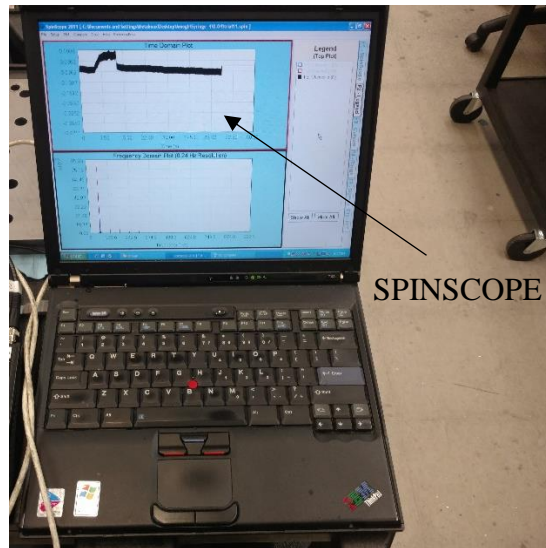


Figure 2-9 SPINSCOPE

2.5.6 DSLR camera

Images of the fluid streams were taken by a Canon EOS Digital SLR camera. It has a 24.2 MP sensor with good focus speed and accuracy; see Figure 2.10.



Figure 2-10 Canon EOS Digital SLR camera [19]

2.6 Procedure

The 3D printed setup was assembled by screwing the post onto the dynamometer and placing the containers on either side of the post as shown in Figure 2.11. Then all the electrical wiring setup was done. Along with using a protective layer of plastic on the dynamometer, the wirings were also covered with bath towels to ensure no water was sprayed on them. The DSLR camera was setup at an appropriate distance (close enough to get a focused image, but not so close as to have water sprayed onto the camera lens) as shown in Figure 2.12.

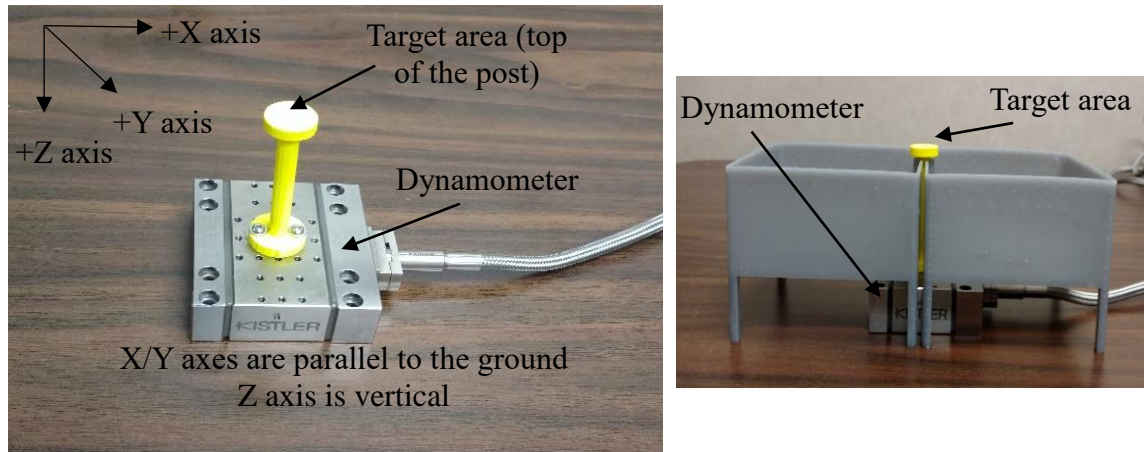


Figure 2-11 3D printed parts and dynamometer setup

The procedural steps followed are represented in the following flowchart.

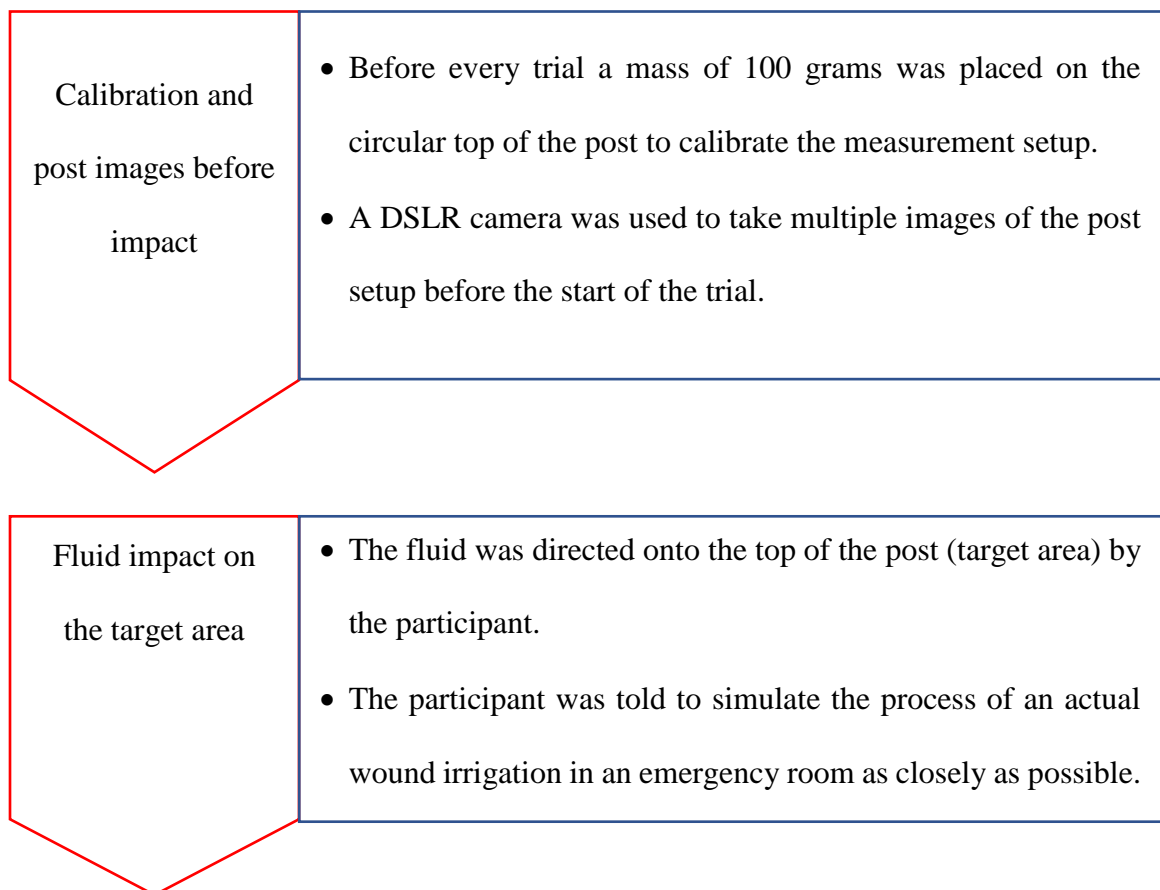


Figure 2-12 Procedure Flowchart

Images taken during impact	<ul style="list-style-type: none">• During the fluid application, multiple images of the stream were captured. The one which most closely represented the process was selected.
Amplifier	<ul style="list-style-type: none">• The amplification of the charge signal output from the dynamometer was done by a Kistler 5814B1 dual mode amplifier.
DAQ	<ul style="list-style-type: none">• DAQ Data Translation DT9837B then digitized the input analog signal for analysis [5].
SPINSCOPE	<ul style="list-style-type: none">• SPINSCOPE, a virtual oscilloscope software was used for visualizing and acquiring the force measurement data.
Force analysis	<ul style="list-style-type: none">• Noise filtering and drift compensation were done on the raw force data to obtain the filtered force data.

Figure 2-12, continued

Stream analysis	<ul style="list-style-type: none">• Image processing tools in MATLAB® R2017a were used to estimate the cross-sectional impact area of the stream or streams.
Pressure calculation	<ul style="list-style-type: none">• The pressure was obtained by dividing the filtered force by the cross-sectional area from the image processing.
Uncertainty evaluation	<ul style="list-style-type: none">• The uncertainty for each measurement was evaluated.

Figure 2-12, continued

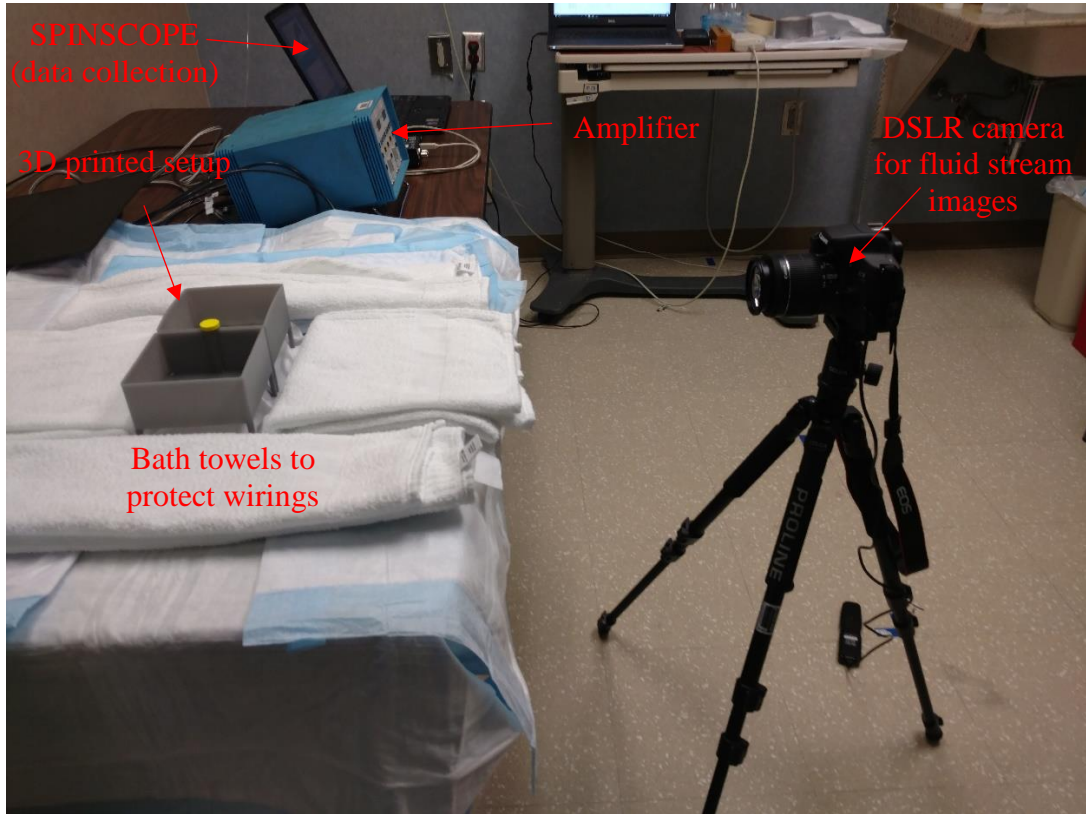


Figure 2-13 Experimental setup (full setup)

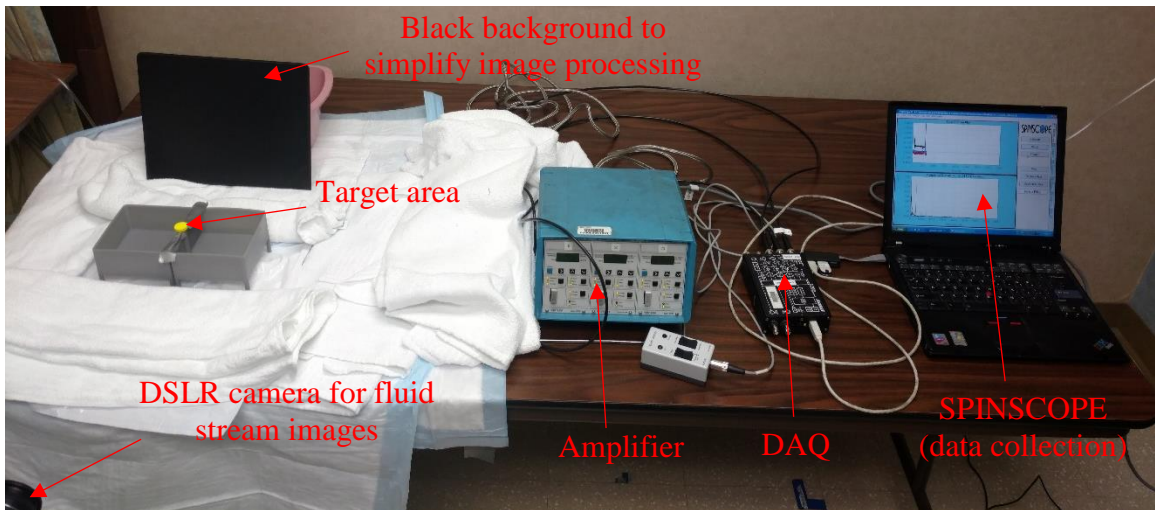


Figure 2-14 Experimental setup (individual views)

3. FORCE DATA ANALYSIS

Force data in the time domain for all 60 trials was extracted from SPINSCOPE and plotted in MATLAB® R2017a.

3.1 High frequency noise

Raw force data in the Z direction for a single trial (participant 13) using the three irrigation devices is shown in Figure 3.1. As seen in the figure, electrical noise was present in the data. Noise can be defined as undesirable electrical signals that interfere with the desired signal [20]. Therefore, to obtain the desired force data, noise suppression or filtering was essential.

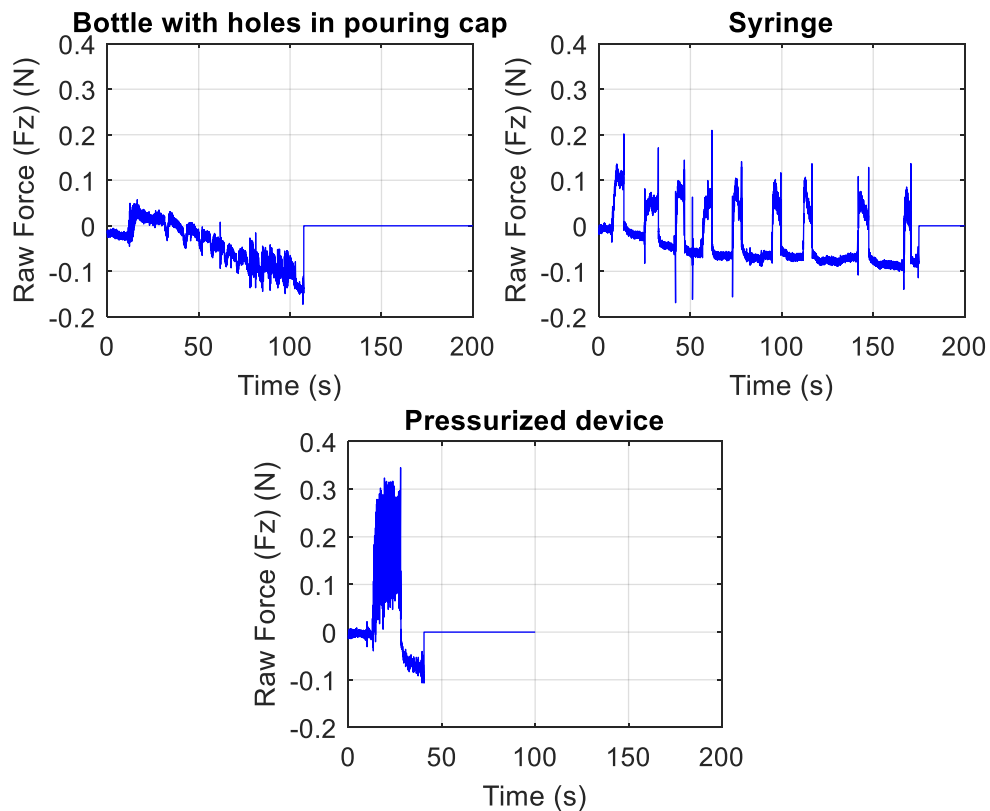


Figure 3-1 Raw force data in the time domain

3.2 Filter selection

Two common methods of filtering data using digital filters are FIR (Finite Impulse Response) and IIR (Infinite Impulse Response). FIR filters use convolution (filter kernels) to filter the signal. IIR filters, or recursion filters, use previously calculated values from the output along with the input points. A recursive filter is defined by a set of constants called recursive coefficients [21]. The Butterworth filter, an IIR filter, was selected for this study. The advantages of using a Butterworth filter are: simplicity of use, 0% ripple, less overshoot, and no ringing.

To see the frequency content of the raw force signal, the time domain raw force data was converted to the frequency domain using the discrete Fourier transform (DFT). This was done by using the ‘fft’ function in MATLAB® R2017a, which uses a fast Fourier Transform (FFT) algorithm to compute the DFT. By observing the force data using the three irrigation devices in the frequency domain (see Figure 3.2), high frequency electrical noise can be seen.

A Butterworth filter function in MATLAB® R2017a (represented by the function ‘butter’) requires three parameters as input: type of filter, normalized cut off frequency, and filter order [22]. Since noise was present at high frequencies (Figure 3.2), a low pass type of Butterworth filter was used.

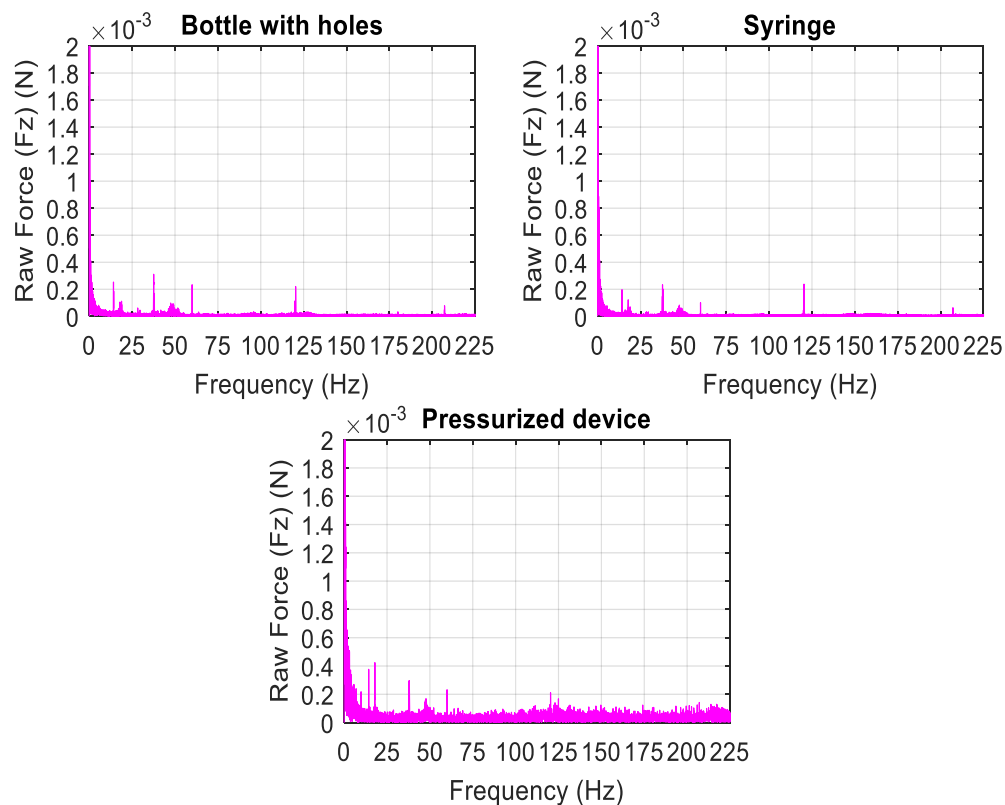


Figure 3-2 Raw force data in the frequency domain

3.2.1 Normalized cut off frequency

The normalized cut off frequency (W_n) is the ratio of cut off frequency (f_c) to half of the sampling frequency (f_s). In signal processing, sampling frequency or sample rate is the number of samples taken per second from the continuous signal. The force signal was sampled at a rate of 2000 samples/sec for all trials in this study.

Time domain force data of a trial conducted without any force (no load) was converted into the frequency domain; see Figure 3.3. The frequency content between Figures 3.2 (irrigation force applied) and 3.3 (no load) is similar. Noise is seen at 60 Hz and its harmonics. These harmonic perturbations are extrinsic noise in the form of power-line noise in the signal at 60 Hz and its harmonics due to alternating current oscillating at

that frequency. Also, content is seen at or near 14 Hz, 17 Hz, 38 Hz, 48 Hz, etc. in all plots. The major difference between the plots is the force present below 1 Hz. In the no load case (Figure 3.3), the amplitude of force present below 1 Hz is less than the force magnitude at the other higher frequencies. This differs from the Figure 3.2 plots in which the force magnitude is much higher at frequencies below 1 Hz than at the other higher frequencies. Therefore, it can be inferred that most of the force signal was present below 1 Hz with mostly noise at frequencies higher than 1 Hz. This was observed in all 60 trials. So, using a cut off frequency of 1 Hz removed most of the noise present in the data without a significant loss of the force signal.

Since the cut off frequency was selected to be 1 Hz and the sampling frequency as 2000 Hz, the normalized cut off frequency for the Butterworth filter function was 0.001.

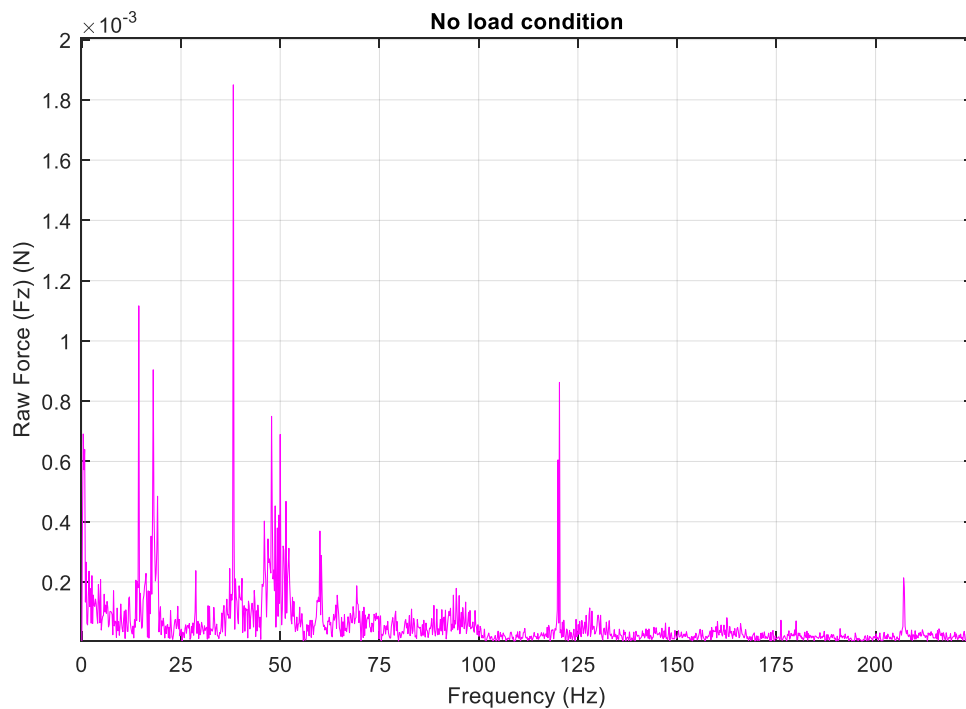


Figure 3-3 Raw force data for no load condition in the frequency domain

3.2.2 Order of the Butterworth filter

The order of a filter is the maximum delay used in calculating an output [23]. The higher the order of the filter, the higher the number of computations per output sample and the sharper the magnitude roll off with increasing frequency. The Butterworth filter function in MATLAB® R2017a returns two vectors as outputs. These are transfer function coefficients 'a' and 'b', where 'a' is a vector that contains all the coefficients of the denominator of the transfer function and 'b' is for the numerator [22]. The number of filter coefficients is greater than the order of the filter by one. Therefore, for example, if the order of the filter is chosen as two, both 'a' and 'b' will be vectors of length three.

For selecting the order of the filter to be used, all orders from one to five were individually used to filter the force data and the output values (recursive coefficients) of 'a' and 'b' were observed. Figure 3.4 shows the filtered force data measurements of participant 13 with the three irrigation devices using orders one to five. It can be seen that increasing the order of the filter to more than three has minimal effect on the filtered signal, so three was selected.

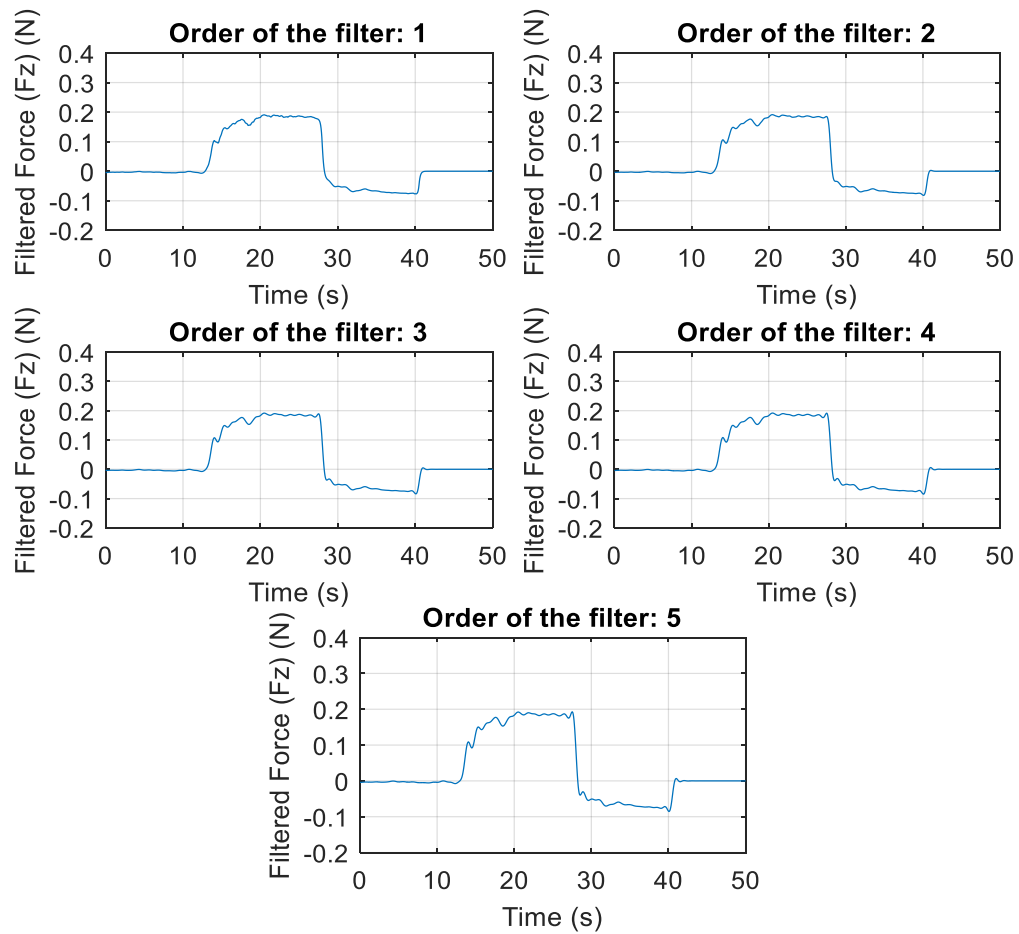


Figure 3-4 Filtered force data measurements with filter order one to five

A 3rd order low pass Butterworth filter with a cut off frequency of 1 Hz was used for filtering the raw force data in all trials. An example of the filtered force data component in the Z direction for all three irrigation devices is shown in Figure 3.5.

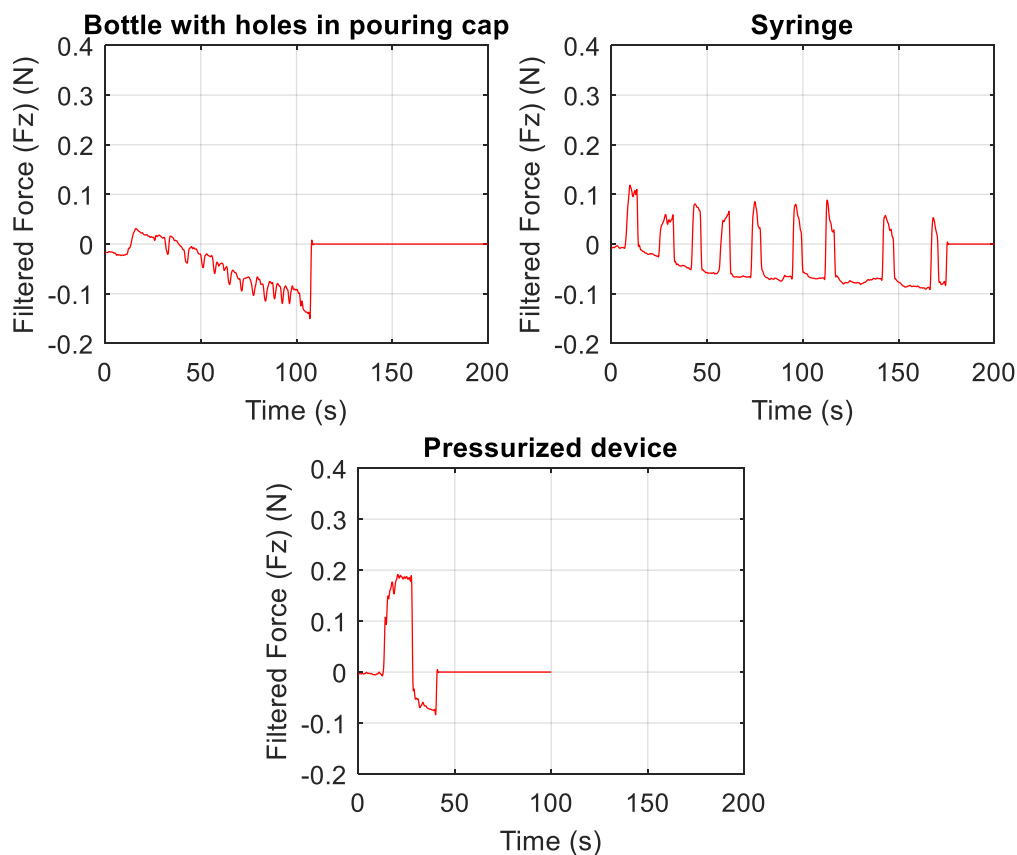


Figure 3-5 Filtered force data (Fz) in the time domain

3.2.3 Drift compensation and DC offset removal

As seen in Figure 3.5, there is drift as well as a DC offset in the filtered data. According to ISA-37.1-1975 (1992), the International Society of Automation standard for electrical transducer nomenclature and terminology, drift can be defined as an undesired change in output over time that is not a function of the measurand [24]. Piezoelectric sensors are known to show a high amount of drift caused by the force to charge conversion [25]. This drift charge is caused by offset voltages and currents in the input circuit of the charge amplifier along with connecting leads and plugs [26]. When using piezoelectric sensors for force measurement the drift of the charge amplifier needs to be considered [27].

In the case of the pressurized irrigation device, the time at which the fluid impact began was taken as the start time and the time at which it ended as the end time. The filtered force data (Figure 3.5) was then truncated to include only data between these two points in time (Figure 3.6).

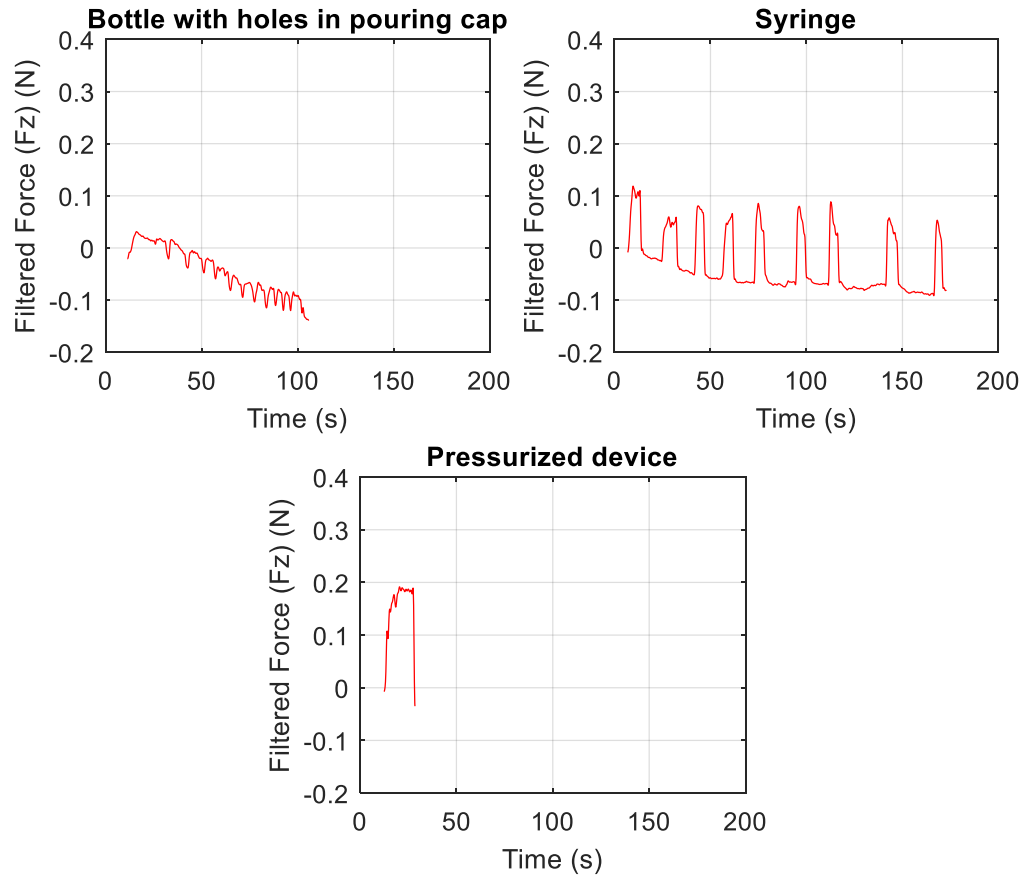


Figure 3-6 Filtered and truncated force data (Fz)

Drift compensation was done by finding the slope of the line passing through these two points and then subtracting that line from the truncated force data set. The ‘polyfit’ and ‘polyval’ functions in MATLAB® R2017a were used to perform this operation. The ‘polyfit’ function was used to find the coefficients of the least squares polynomial generated for the truncated force data. Next, the ‘polyval’ function was used to generate a

curve/slope to fit the truncated force data using the 'polyfit' coefficients. This slope was then subtracted from the filtered truncated force data.

For irrigation devices 1 and 2, i.e., the bottle with four holes punctured in the pouring cap and the syringe, respectively, the fluid impact starts and stops many times during a single trial. For these two irrigation devices the filtered force data was divided into segments with each segment defined between consecutive start and stop times. Using 'polyfit' and 'polyval' functions the slope removal process was done individually for all segments.

As can be observed in Figure 3.5, there is a variation in the force value at the start point of the truncated force data. This DC offset also needed to be removed. To remove this offset, the variation of the force value at the start point was subtracted from the force data, i.e., the entire force measurement data was shifted so that the force data value at the start point zero. Figure 3.7 shows the filtered force component (F_z) with drift compensation and DC offset removal for the three irrigation devices.

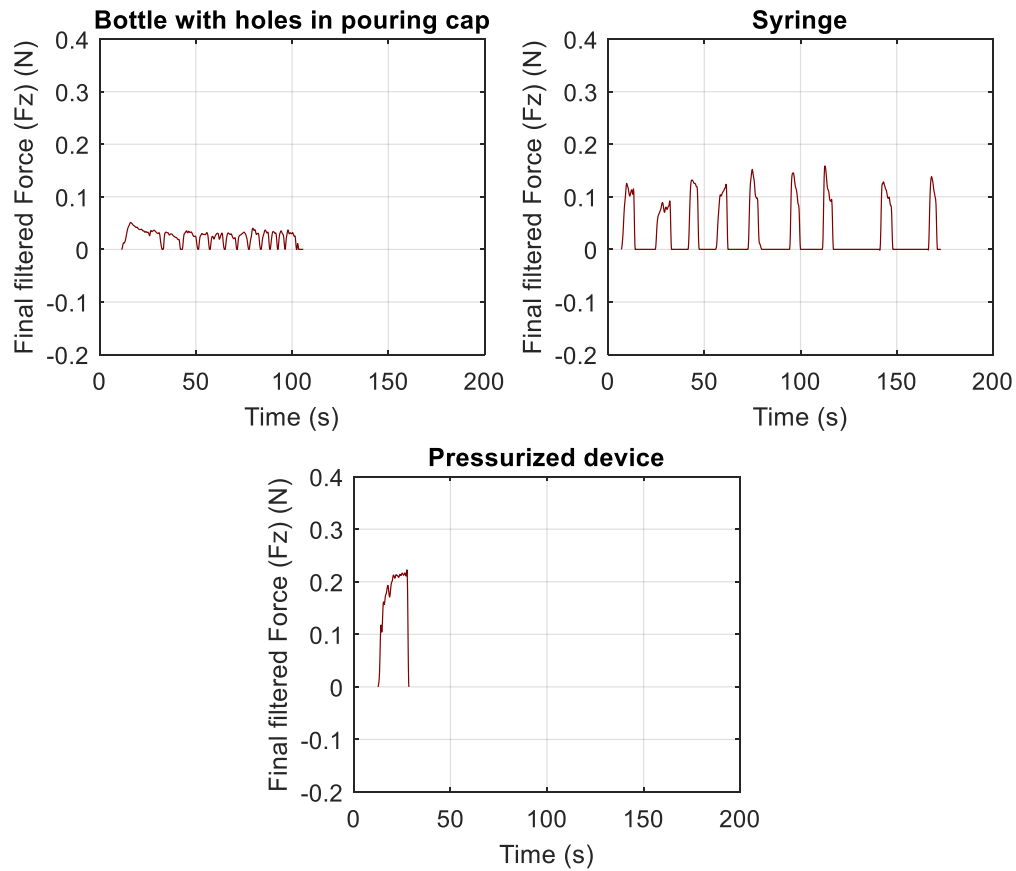


Figure 3-7 Final filtered force data with slope and offset removal

3.3 Resultant force calculation for all 60 trials

Noise filtering, slope removal, and DC offset removal was done for the raw force in all three directions separately (F_x , F_y , and F_z). The components were then combined as shown in Equation 3.1 to obtain the resultant force. The same process was followed for all 60 trials.

$$F = \sqrt{F_x^2 + F_y^2 + F_z^2} \quad (3.1)$$

where,

F_x = Force component in the x direction

F_y = Force component in the y direction

F_z = Force component in the z direction

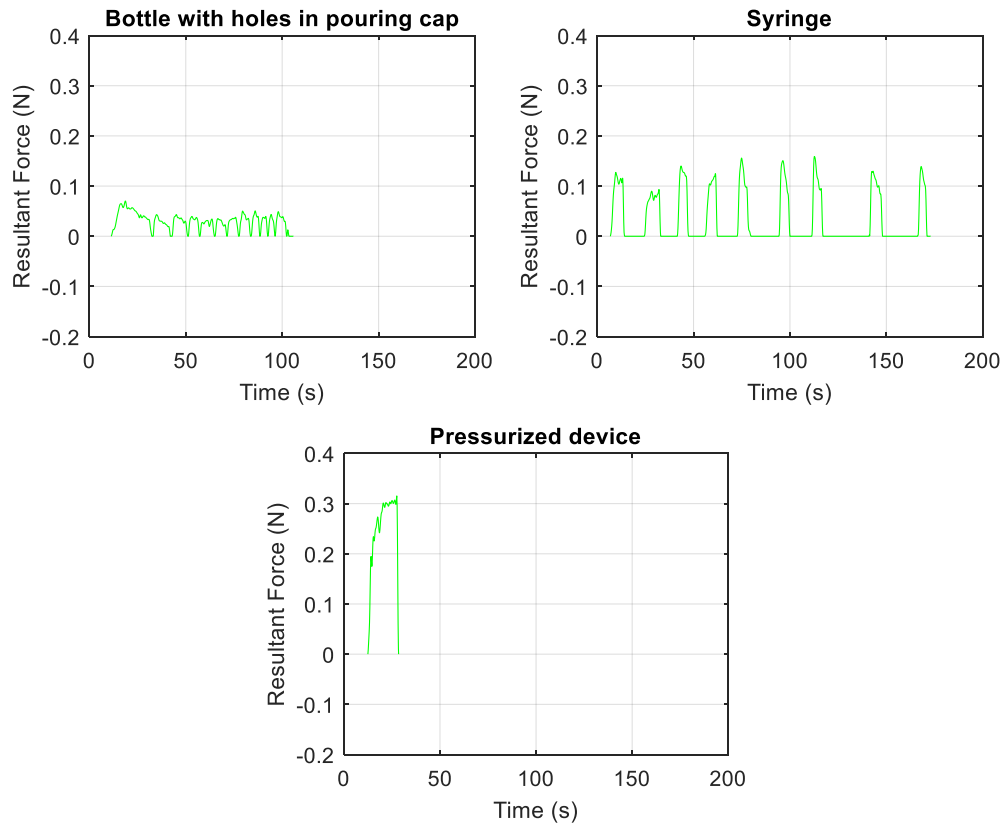


Figure 3-8 Final resultant force data (F)

4. STREAM AREA ANALYSIS

The cross-sectional impact area of the fluid stream was estimated by locating the edges of the stream close to the point of impact. The distance between the edges provided the diameter of the impact area which in turn was converted into the cross-sectional area of the fluid. Locating the stream edges was completed using various image processing tools in MATLAB® R2017a.

4.1 Selection of an edge detection tool

Image segmentation is the partitioning of an image into multiple regions using discontinuities in that image [28]. Edges are characterized by rapid intensity changes in an image or sharp discontinuities in an image. Edge detection, which is the primary step in image segmentation, is the process of identifying and locating these edges [28, 29]. There are numerous methods of edge detection, including Sobel filtering, Prewitt filtering, and Canny edge detection [30]. Canny edge detection [31] is an optimal edge detection technique which provides good detection and localization of thin edges and smooth continuous pixels [32, 33]. For images with reasonably similar content (as is the case in these trials), a well-tuned canny edge detector is a good option [32]. Hence, a canny edge was selected as the edge detection algorithm for this study.

4.2 Preprocessing before canny edge detection

Of multiple images taken during a trial, an image which best represented the process was selected and input in MATLAB® R2017a. Initially, the original selected image taken during a trial was cropped to focus on the stream since only the stream was the area of concern; an example is shown in Figure 4.1. This made it easier to locate edges. The first

pre-processing step when using a canny edge detector is the reduction of high frequency noise. The presence of noise in an image makes locating edges difficult.

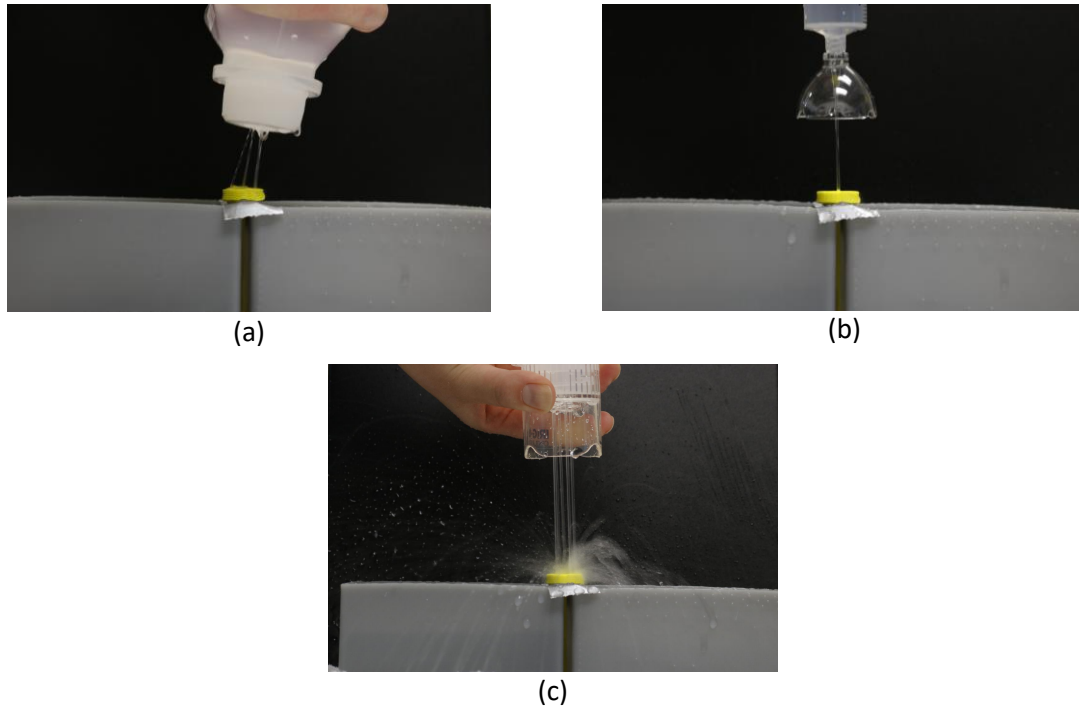


Figure 4-1 Irrigation device images taken by a DSLR camera during fluid impact: (a) bottle with four holes in pouring cap; (b) syringe; (c) pressurized device.

A two-dimensional Gaussian smoothing function was used to reduce noise present in the cropped image. A Gaussian filter is a low pass filter that works by convolving the image with a Gaussian kernel which smooths the image [34]. In MATLAB® R2017a, the function ‘imgaussfilt’ represents a 2D Gaussian function. The input to a Gaussian smoothing function is a grayscale image, so the cropped image was initially converted to a grayscale image. The smoothing of the Gaussian filter is controlled by the parameter ‘ σ ’ or standard deviation. Sharp edges are characterized by high intensity changes. As standard deviation parameter (σ) of the filter is increased, these rapid intensity changes become smoother. The localization error in the detected edges also increases slightly as the

Gaussian width is increased [35]. Therefore, a standard deviation value of 1 was selected as optimal for detection of edges with the removal of high frequency noise.

Another pre-processing step before the use of a canny edge detection function is the use of a contrast enhancement technique. Using the function 'imadjust' in MATLAB® R2017a, the contrast of the image was enhanced to make it clearer for visualization.

4.3 Canny edge detection

In MATLAB® R2017a, the inputs required for a canny edge detector function are: σ and threshold. σ is the standard deviation of the Gaussian filter used in the canny function. Based on the σ value, the size of the filter is automatically chosen.

Thresholding (intensity based segmentation) is a simple method of image segmentation. It converts a grayscale image into a binary image by converting all pixel values to either zero or one, depending on the threshold value. There are different methods of thresholding used in edge detection. In the case of canny edge detection, the hysteresis technique of thresholding is used. Hysteresis thresholding specifies two threshold values: a low threshold value and a high threshold value. Anything below the low threshold is discounted since it is not a strong enough response, while anything above the high threshold is counted since it is a strong response edge. Any edge in between both the thresholds are preserved only if it is connected to a strong response edge which is above the high threshold.

There are various methods of auto selecting the threshold values, including the iterative selection algorithm, the entropy based method, Otsu's method, statistical models, and others [36, 37, 38]. Otsu's method [39] was used to find the threshold values to be

input into the canny edge detector. In MATLAB® R2017a, the ‘graythresh’ function uses Otsu’s method to compute the global threshold value. The ‘graythresh’ function returns the high threshold value which can be directly input into the canny edge detector. Typically, as shown in equation 4.1, the low threshold value is taken as half of the high threshold value [37]; this value was selected here as well. Unlike the threshold value inputs to the canny operator, the σ input was not taken as a standard value for all trials. Having a high σ value decreases the noise, but increases the possibility of losing useful edge information [37]. Therefore, the σ value was modified for every image and the σ value was selected for which the clearest edge was detected.

Examples of the edge detection results (participant 13) are shown in Figures 4.2, 4.3, and 4.4 for the three irrigation devices, respectively. The impact area representations are shown in red. The same process of edge detection was applied for locating the edges of the top of the post. An example is shown in Figure 4.5. Following the same procedure, the edges of the stream and the post top were located for all 60 trial images.

$$T_1 = 0.5 \times T_2 \quad (4.1)$$

where,

T_1 = High threshold value

T_2 = Low threshold value

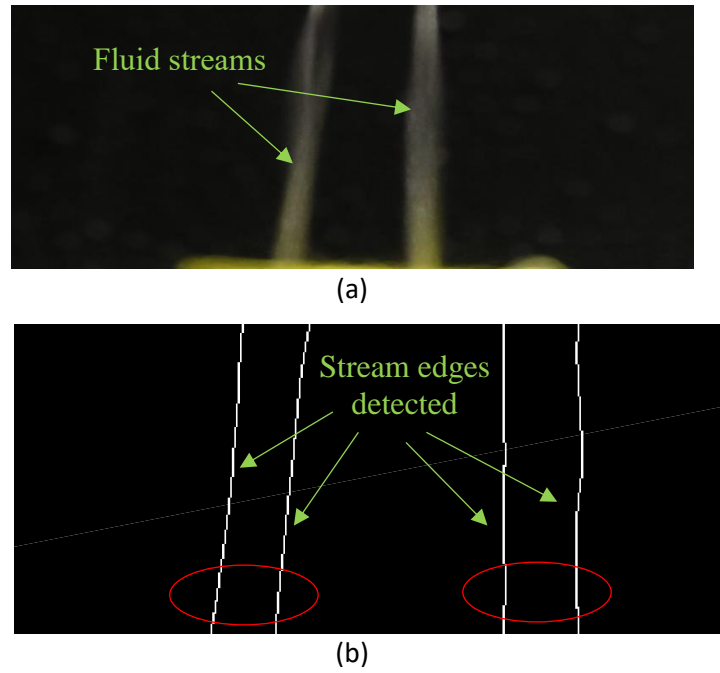


Figure 4-2 (a) before edge detection for participant 13 using the bottle with four holes in pouring cap; (b) after edge detection for participant 13 using the bottle with four holes in pouring cap

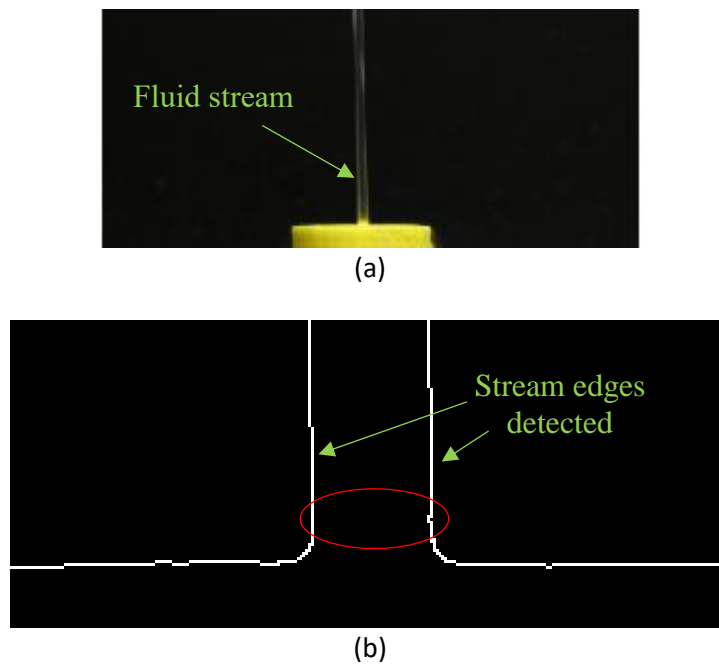
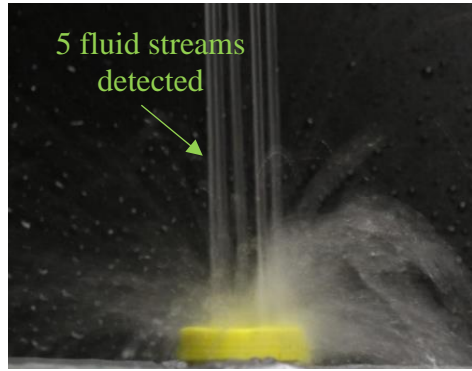
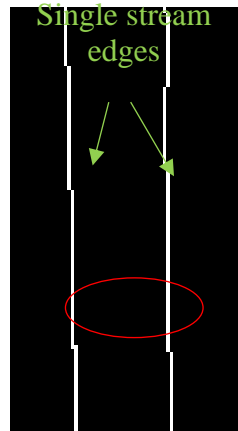


Figure 4-3 (a) before edge detection for participant 13 using the syringe; (b) after edge detection for participant 13 using the syringe



(a)

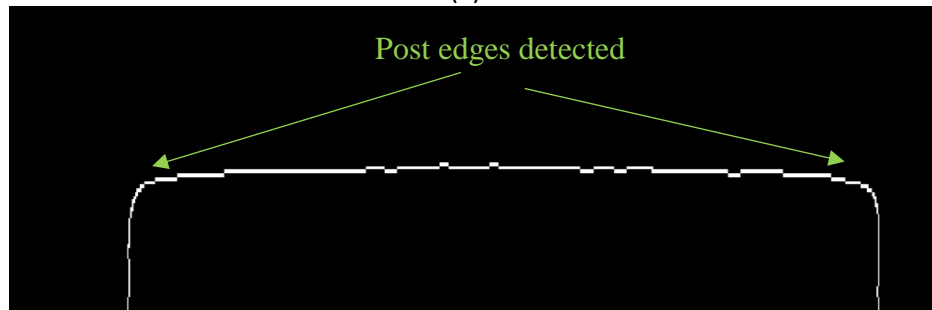


(b)

Figure 4-4 (a) before edge detection for participant 13 using the pressurized device; (b) after edge detection for participant 13 using the pressurized device



(a)



(b)

Figure 4-5 (a) before edge detection of the post for participant 13; (b) after edge detection of the post for participant 13

4.4 Stream impact area calculation

Since the edges of the stream/streams and the edges of the post were located, the number of pixels between the edges of a single stream (p_d) were calculated along with the number of pixels between the post top edges (p_D). Also, using a digital Vernier caliper (Mitutoyo CD-6 ASX), the diameter of the post (D) was measured. A ratio of the pixel count of the stream and the pixel count of the post top was taken and then compared with the ratio of the diameter of the stream (d) and the diameter of the top of the post. Using Equations 4.2, the diameter of the stream was found for the three irrigation devices (shown in Equations 4.3, 4.5, and 4.7, respectively).

$$\frac{p_d}{p_D} = \frac{d}{D} \quad (4.2)$$

4.4.1 Impact fluid area for bottle with four holes in the pouring cap (irrigation device 1)

For this irrigation device there are two impact streams even though there are 4 holes through which the fluid flows out of the bottle. This is due to the merging of the streams into only two streams before the fluid impacts the impact area. The impact area of the streams was calculated by first finding the average diameter of the impact stream from Equation 4.3 and then the total impact stream area using Equation 4.4 (the factor of 2 is included to consider both streams).

$$d_1 = \frac{D p_{d1}}{p_{D1}} \quad (4.3)$$

where,

d_1 = average diameter of a single impact fluid stream

p_{d1} = average pixel count of the impact stream

D = diameter of the post top/target area

p_{D1} = average pixel count of the post top between edges

$$A_1 = 2\pi \left(\frac{d_1}{2} \right)^2 \quad (4.4)$$

where,

A_1 = total impact area of fluid streams

d_1 = average diameter of a single fluid stream

4.4.2 Impact fluid area with syringe (irrigation device 2)

The syringe has a single impact stream. Equations 4.5 and 4.6 were used to calculate the diameter of the impact stream and total area of the impact stream, respectively.

$$d_2 = \frac{Dp_{d2}}{p_{D2}} \quad (4.5)$$

where,

d_2 = diameter of the impact fluid stream

p_{d2} = pixel count of the impact stream

D = diameter of the post top

p_{D2} = pixel count of the post top between edges

$$A_2 = \pi \left(\frac{d_2}{2} \right)^2 \quad (4.6)$$

where,

A_2 = total impact area of the fluid stream

d_2 = diameter of the fluid stream

4.4.3 Impact fluid area with pressurized irrigation device (irrigation device 3)

For the pressurized irrigation device, there are five streams which impact the post top and so the total impact surface area (A) is five times the single stream area (shown in Equation 4.7).

$$d_3 = \frac{Dp_{d3}}{p_{D3}} \quad (4.7)$$

where,

d_3 = diameter of a single impact fluid stream

p_{d3} = pixel count of a single impact stream

D = diameter of the post top

p_{D3} = pixel count of the post top between edges

$$A_3 = 5\pi \left(\frac{d_3}{2} \right)^2 \quad (4.8)$$

where,

A_3 = total impact area of the five fluid streams

d_3 = diameter of a single fluid impact stream

Similarly, using the previous equations the impact area for all 20 participants using the three irrigation devices was found (60 trials).

5. PRESSURE CALCULATION

The time-dependent fluid stream pressure was calculated by dividing the time-dependent force by the total stream impact area. This was done for each participant using all three irrigation devices. An example plot for a single participant is displayed in Figure 5.1.

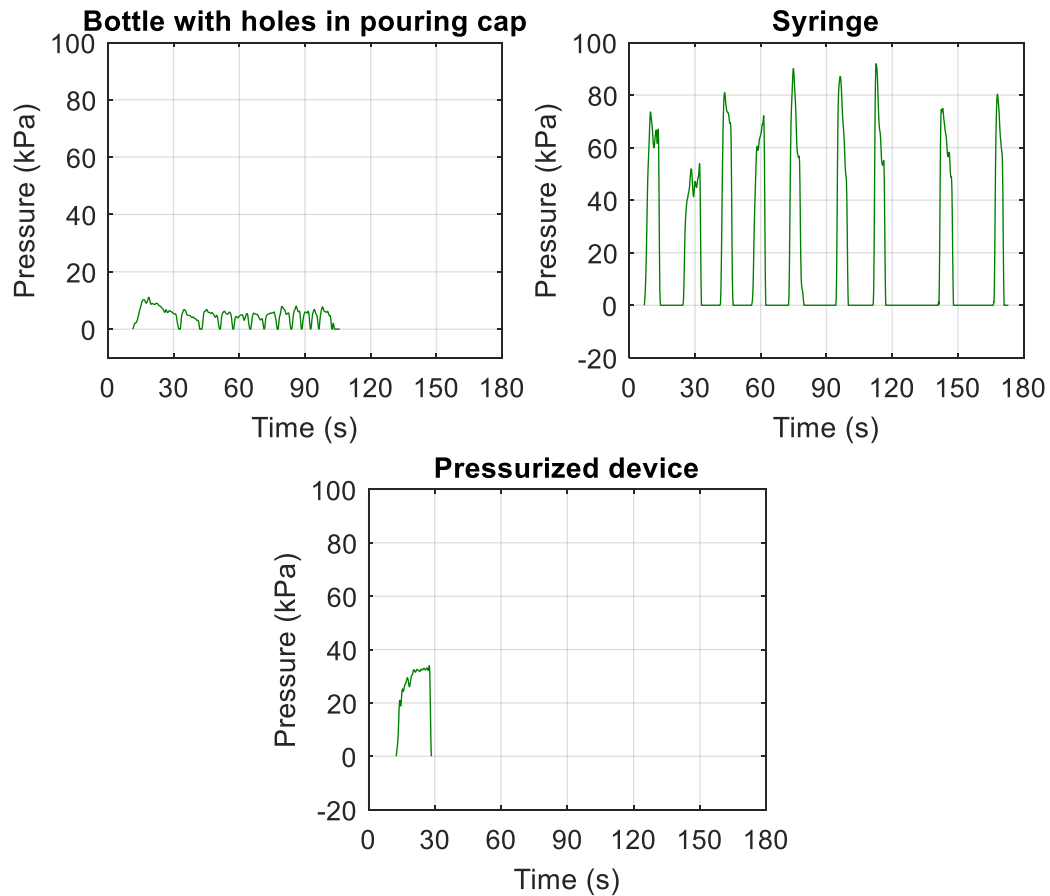


Figure 5-1 Pressure vs. time for participant 13 using the three irrigation devices

For the bottle, the force was divided by the area of the two final streams. The syringe pressure was the force divided by the single stream area. The pressurized device pressure was determined by dividing the force by the sum of the five streams. It is seen that the bottle pressure oscillates as the user squeezes the bottle, releases it to allow air to replace

the fluid volume lost, and then squeezes it again. A similar result is observed for the syringe, where it was refilled nine total times to dispense the full 500 ml of irrigation fluid. A single, approximately constant pressure record is seen for the pressurized device because no interruption from the user is required to dispense the total volume of fluid.

6. UNCERTAINTY ANALYSIS

Every measured quantity has an associated uncertainty. It is essential to evaluate this uncertainty in order to fully describe the measurement result.

6.1 Propagation of uncertainty

In these experiments, pressure was calculated from the measured force and stream area near the point of impact. By the law of propagation of uncertainty, the combined standard uncertainty of the dependent variable or measurand (fluid stream pressure in this case) can be determined by combining the uncertainties in the independent variables (force due to fluid impact and total stream impact area). The pressure equations for the three irrigation devices are provided in the following paragraphs.

6.1.1 500 ml bottle with four holes in pouring cap (irrigation device 1)

From Equation 4.3 and Equation 4.4, the total impact area of the four streams for irrigation device 1 is given by,

$$A_1 = 2\pi \left(\frac{d_1}{2} \right)^2 = 2\pi \left(\frac{D p_{d1}}{2 p_D} \right)^2 \quad (6.1)$$

where,

A_1 = total impact area of fluid streams for irrigation device 1

d_1 = average diameter of a single fluid stream

D = diameter of the post top/target area

p_{d1} = average pixel count of the impact streams

p_D = pixel count of the post top diameter

Substituting Equation 6.1 in Equation 2.1 gives,

$$P_1 = \frac{F_1}{A_1} = \frac{F_1}{2\pi \left(\frac{Dp_{d1}}{2p_D} \right)^2} = \frac{2F_1 p_D^2}{\pi D^2 p_{d1}^2} \quad (6.2)$$

where,

P_1 = time-dependent fluid stream pressure by irrigation device 1

F_1 = time-dependent force

6.1.2 60 ml syringe (irrigation device 2)

The total impact area of the fluid stream for the syringe device obtained from Equations 4.5 and 4.6 is,

$$A_2 = \pi \left(\frac{d_2}{2} \right)^2 = \pi \left(\frac{Dp_{d2}}{2p_D} \right)^2 \quad (6.3)$$

where,

A_2 = total impact area of the fluid stream by irrigation device 2

d_2 = diameter of the impact fluid stream

p_{d2} = pixel count of the impact stream

Substituting Equation 6.3 in Equation 2.1 gives,

$$P_2 = \frac{F_2}{A_2} = \frac{F_2}{\pi \left(\frac{Dp_{d2}}{2p_D} \right)^2} = \frac{4F_2 p_D^2}{\pi D^2 p_{d2}^2} \quad (6.4)$$

where,

P_2 = time-dependent fluid stream pressure by irrigation device 2

F_2 = time-dependent force

6.1.3 Pressurized irrigation device (irrigation device 3)

From Equation 4.7 and Equation 4.8, the total impact area of the fluid stream for the pressurized irrigation device is,

$$A_3 = 5\pi \left(\frac{d_3}{2} \right)^2 = 5\pi \left(\frac{Dp_{d3}}{2p_D} \right)^2 \quad (6.5)$$

where,

A_3 = total impact area of the fluid streams for irrigation device 3

d_3 = diameter of the impact fluid stream

p_{d3} = pixel count of the impact stream

Substituting Equation 6.3 in Equation 2.1, we get

$$P_3 = \frac{F_3}{A_3} = \frac{F_3}{5\pi \left(\frac{Dp_{d3}}{2p_D} \right)^2} = \frac{4F_3 p_D^2}{5\pi D^2 p_{d3}^2} \quad (6.6)$$

where,

P_3 = time-dependent fluid stream pressure by irrigation device 3

F_3 = time-dependent force

p_{d3} = pixel count of the impact stream

6.2 Combined standard uncertainty

As per GUM [40], the combined standard uncertainty of a measurand which is influenced by the uncertainties of different input parameters, is described as the square root of the sum of the products of squares of the individual parameter uncertainties and the squares of the sensitivity coefficients associated with them. The correlation between input parameters has been taken to be zero.

$$u_c = \sqrt{\sum_i c_i^2 u_i^2} \quad (6.7)$$

where,

u_c = combined standard uncertainty

c_i = sensitivity coefficient

u_i = input standard uncertainty

6.2.1 Calculation of mean values of independent quantities

All partials were evaluated at the mean pressure for each measurement. The method for calculating the mean values of the input quantities (F , D , p_D , p_d) is described in the following paragraphs, where F is the time-dependent force, D is the diameter of the post top, p_D is the pixel count from the post top image, and p_d is the pixel count from the stream image.

In the case of F , the following steps were used. First, the time interval for the applied pressure was determined. For the pressurized device there is single interval per trial. For the bottle and syringe, however, there were multiple intervals. In all cases, the interval was identified by two points based on the start and end points (see Figures 6.1-6.3 from participant 13). The force data for the interval was truncated to contain only force data between these start and end points. The mean force value of the trial was then calculated by taking the mean value of the truncated force data. Equation 6.8 (irrigation device 3) shows the mean calculation for the pressurized device. Equation 6.9 and Equation 6.10 present the mean force for the bottle (irrigation device 1) and syringe (irrigation device 2).

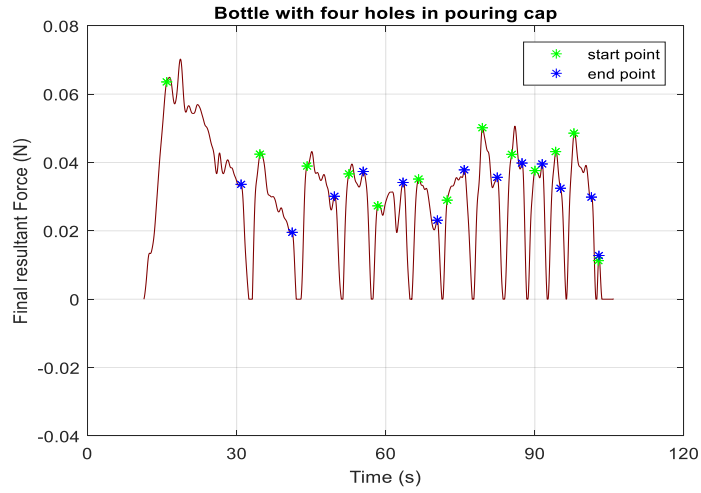


Figure 6-1 Bottle with four holes in pouring cap

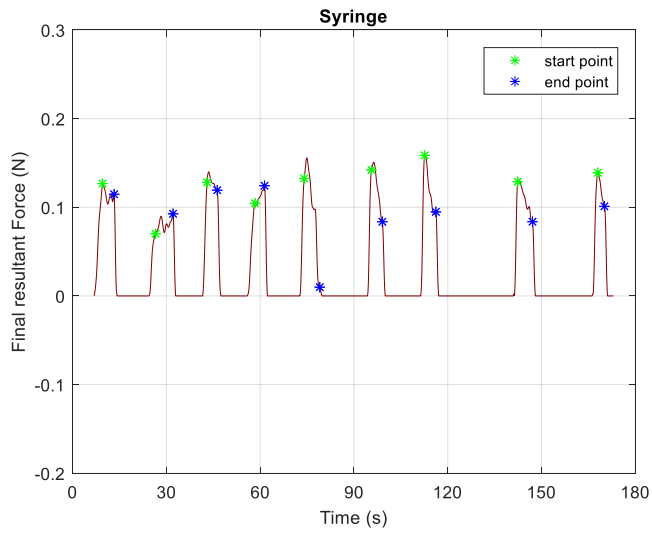


Figure 6-2 Syringe

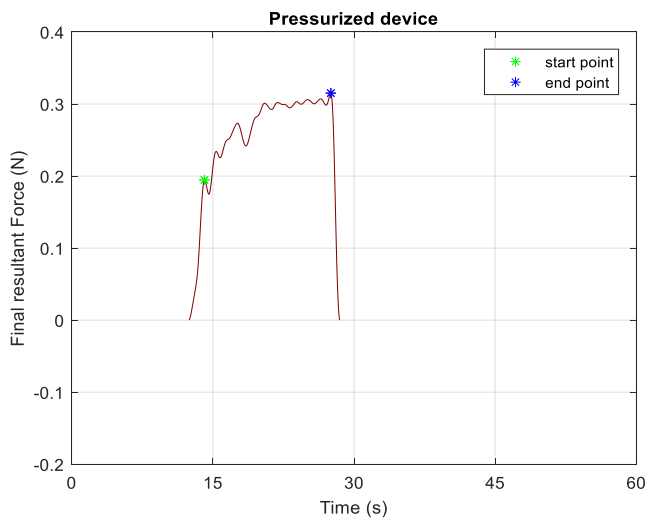


Figure 6-3 Pressurized device

$$F_{m3} = \bar{x}(F_{t3}) \quad (6.8)$$

where,

F_{m3} = mean force value of the truncated force data

F_{t3} = truncated force data

$$F_{m1} = \bar{x}(\bar{x}(F_{t1}), \bar{x}(F_{t2}), \dots, \bar{x}(F_{tn})) \quad (6.9)$$

where,

F_{m1} = mean force value from all intervals

$F_{t1}, F_{t2}, \dots, F_{tn}$ = truncated force data from n intervals

$$F_{m2} = \bar{x}(\bar{x}(F_{t1}), \bar{x}(F_{t2}), \dots, \bar{x}(F_{tn})) \quad (6.10)$$

where,

F_{m2} = mean force value form all intervals

$F_{t1}, F_{t2}, \dots, F_{tn}$ = truncated force data from n intervals

The the diameter of the post top (D) was measured using a digital Vernier caliper (Mitutoyo CD-6 ASX). This was taken as the mean value.

In the case of p_D , the number of pixels between the edges of the post top diameter was taken as the mean value.

The mean value of p_d was found by counting the number of pixels between the edges of the fluid stream or taking the average number of pixels in the case of multiple fluid streams.

Mean values of all 20 participants for the three irrigation devices are shown in Table 6.1.

Table 6-1 Mean values of independent variables

Participant	Mean values								
	Bottle with four holes			Syringe			Pressurized device		
	F_{m1} (N)	p_D	p_{d1}	F_{m2} (N)	p_D	p_{d2}	F_{m3} (N)	p_D	p_{d3}
1	0.057	852.5	92.1	0.111	849.7	66.8	0.200	848.2	81.5
2	0.032	528.8	44.6	0.114	534.0	34.1	0.170	399.3	37.4
3	0.028	559.8	51.3	0.080	564.1	33.4	0.148	349.1	30.7
4	0.051	554.3	45.0	0.081	556.0	37.0	0.186	345.2	31.4
5	0.028	560.8	58.1	0.114	560.9	39.8	0.276	359.8	32.0
6	0.031	531.0	51.0	0.077	527.4	30.4	0.133	353.0	32.7
7	0.039	542.1	50.5	0.129	542.9	39.0	0.269	346.2	32.7
8	0.060	524.5	38.2	0.114	519.7	32.4	0.162	363.0	36.8
9	0.042	557.5	39.3	0.087	561.2	36.2	0.188	382.5	31.5
10	0.041	562.0	34.3	0.090	566.6	40.3	0.252	362.4	34.6
11	0.051	543.2	45.7	0.069	544.2	37.3	0.233	372.0	32.0
12	0.019	572.0	47.2	0.093	579.0	47.1	0.148	357.5	31.6
13	0.035	496.0	41.8	0.113	502.7	38.7	0.197	335.2	26.7
14	0.024	469.1	32.1	0.089	464.8	32.6	0.190	336.6	31.6
15	0.075	455.0	28.3	0.134	454.6	31.5	0.269	316.4	27.8
16	0.028	469.8	42.8	0.156	470.0	33.1	0.151	305.1	30.1
17	0.024	470.0	31.3	0.104	475.6	36.3	0.184	321.7	29.0
18	0.035	463.9	38.9	0.111	468.8	29.2	0.195	329.0	28.4
19	0.058	475.0	31.5	0.258	476.0	33.0	0.239	315.1	26.4
20	0.028	480.4	46.1	0.134	480.1	36.9	0.101	328.4	29.6

6.2.2 Sensitivity coefficients (c_i)

Sensitivity coefficients (c_i) are determined by taking the partial derivatives of the model function (P in this case) with respect to the input quantities (F , D , p_D , p_d). For the bottle with four holes in the pouring cap, the sensitivity coefficients are calculated by Equations 6.11-6.14,

$$\frac{\partial P_1}{\partial F_1} = \frac{2p_D^2}{\pi D^2 p_{d1}^2} \quad (6.11)$$

$$\frac{\partial P_1}{\partial D} = -\frac{4F_1 p_D^2}{\pi D^3 p_{d1}^2} \quad (6.12)$$

$$\frac{\partial P_1}{\partial p_D} = -\frac{4F_1 p_D}{\pi D^2 p_{d1}^2} \quad (6.13)$$

$$\frac{\partial P_1}{\partial p_{d1}} = -\frac{4F_1 p_D^2}{\pi D^2 p_{d1}^3} \quad (6.14)$$

For the syringe device, the sensitivity coefficients are calculated by Equations 6.15-6.18,

$$\frac{\partial P_2}{\partial F_2} = \frac{4p_D^2}{\pi D^2 p_{d2}^2} \quad (6.15)$$

$$\frac{\partial P_2}{\partial D_2} = \frac{8F_2 p_D^2}{\pi D^2 p_{d2}^2} \quad (6.16)$$

$$\frac{\partial P_2}{\partial p_D} = -\frac{8F_2 p_D^2}{\pi D^3 p_{d2}^2} \quad (6.17)$$

$$\frac{\partial P_2}{\partial p_{d2}} = -\frac{8F_2 p_D^2}{\pi D^2 p_{d2}^2} \quad (6.18)$$

For the pressurized irrigation device, the sensitivity coefficients are calculated by Equations 6.17-6.20,

$$\frac{\partial P_3}{\partial F_3} = \frac{4p_D^2}{5\pi D^2 p_{d3}^2} \quad (6.17)$$

$$\frac{\partial P_3}{\partial D} = \frac{8F_3 p_D}{5\pi D^2 p_{d3}^2} \quad (6.18)$$

$$\frac{\partial P_3}{\partial p_D} = -\frac{8F_3 p_D^2}{5\pi D^3 p_{d3}^2} \quad (6.19)$$

$$\frac{\partial P_3}{\partial p_{d3}} = -\frac{8F_3 p_D^2}{5\pi D^2 p_{d3}^3} \quad (6.20)$$

The sensitivity coefficient values for all trials were calculated and are provided in Tables 6.2-6.7.

6.2.3 Standard uncertainty (u_i)

A standard uncertainty (u_i) is taken from the standard deviation of the corresponding inputs. The inputs were F , D , p_D , and p_d .

The uncertainty in F was calculated from the noise floor of the force data. As shown in Figures 6.4-6.6, the force data was truncated between the start of the sampling time and the start of the force interval. The standard deviation of these values was calculated and taken to be the uncertainty in F .

$$u(F) = \sigma(F_{nt}) \quad (6.21)$$

where,

$u(F)$ = force standard uncertainty

F_{nt} = noise floor force values

σ = standard deviation

The uncertainty in D was obtained from the specifications for the digital Vernier caliper (Mitutoyo CD-6 ASX) [41] since it was used for the measurement of the diameter of the top of the post (target area). The value represented as ‘accuracy’ was taken to be the standard uncertainty in D .

The uncertainty in p_D was determined by first calculating the pixel count of 10 rows of values between post top edges at the impact point of the stream. The standard deviation of this range in pixel count values was taken as the standard uncertainty.

$$u(p_D) = \sigma(p_{Dr1}, p_{Dr2}, \dots, p_{Dr10}) \quad (6.22)$$

where,

p_D = pixel count of the post diameter

$p_{Dr1}, p_{Dr2}, \dots, p_{Dr10}$ = pixel counts of the post diameter

The uncertainty in p_d was determined by first calculating the pixel count of a range of values as close as possible to the impact point of the stream. The standard deviation of this range of pixel count values was taken as the standard uncertainty.

$$u(p_d) = \sigma(p_{dr1}, p_{dr2}, \dots, p_{dr10}) \quad (6.23)$$

where,

p_d = pixel count of the stream diameter

$p_{dr1}, p_{dr2}, \dots, p_{dr10}$ = pixel counts of the stream diameter

The standard uncertainty values for all trials using the three irrigation devices were calculated and are provided in Table 6.2-6.7.

Substituting the sensitivity coefficient values and the standard uncertainties, the combined standard uncertainty can be written as,

$$u_c(P) = \sqrt{\left(\frac{\partial P}{\partial F}\right)^2 u^2(F) + \left(\frac{\partial P}{\partial D}\right)^2 u^2(D) + \left(\frac{\partial P}{\partial p_D}\right)^2 u^2(p_D) + \left(\frac{\partial P}{\partial p_d}\right)^2 u^2(p_d)}$$

where,

$$\frac{\partial P}{\partial F} = \text{sensitivity coefficient associated with } F$$

$$\frac{\partial P}{\partial D} = \text{sensitivity coefficient associated with } D$$

$$\frac{\partial P}{\partial p_D} = \text{sensitivity coefficient associated with } p_D \quad (6.24)$$

$$\frac{\partial P}{\partial p_d} = \text{sensitivity coefficient associated with } p_d$$

$$u(F) = \text{standard uncertainty in } F$$

$$u(D) = \text{standard uncertainty in } D$$

$$u(p_D) = \text{standard uncertainty in } p_D$$

$$u(p_d) = \text{standard uncertainty in } p_d$$

6.3 Expanded uncertainty

The expanded uncertainty (U) is obtained by multiplying the combined standard uncertainty (u_c) by a coverage factor (k). A coverage factor of 2 was selected here.

$$U(P) = k u_c(P)$$

where,

$$U(P) = \text{Expanded uncertainty of mean fluid pressure} \quad (6.25)$$

$$k = \text{coverage factor}$$

$$u_c(P) = \text{combined standard uncertainty of mean fluid pressure}$$

The expanded uncertainty values for the 20 participants using the three irrigation devices was calculated and tabulated (see Table 6.2-6.7).

Table 6-2: Combined uncertainty and expanded uncertainty values using bottle with four holes in pouring cap for first 10 participants

Participant	Standard uncertainties				Sensitivity coefficients				Combined standard uncertainty	Expanded uncertainty
	$u(F_1)$ (N)	$u(p_D)$	$u(p_{dl})$	$u(D)$ (m)	dP_1/dF_1	dP_1/dp_D	dP_1/dp_{dl}	dP_1/dD		
1	0.0030	0.5270	0.5271	5.08x10 ⁻⁵	146370.9933	19.4864	-180.3708	-860554.9600	0.46	0.92
2	0.0034	0.4216	0.8355	5.08x10 ⁻⁵	96279.3108	15.5435	-184.4980	-425786.7731	0.37	0.73
3	0.0064	0.4216	0.4523	5.08x10 ⁻⁵	81531.1457	8.1290	-88.7928	-235735.1927	0.52	1.05
4	0.0019	1.4181	0.0000	5.08x10 ⁻⁵	103683.6378	18.9484	-233.4016	-544087.8398	0.20	0.41
5	0.0010	0.4216	0.5483	5.08x10 ⁻⁵	63775.9679	8.9756	-86.7100	-260749.8525	0.08	0.16
6	0.0013	0.0000	0.5217	5.08x10 ⁻⁵	74224.3088	8.6822	-90.4859	-238823.8947	0.11	0.21
7	0.0064	0.3162	0.3334	5.08x10 ⁻⁵	78744.7403	11.3849	-122.2130	-319713.8893	0.50	1.00
8	0.0014	0.8498	0.2582	5.08x10 ⁻⁵	128827.8490	29.5511	-405.7476	-802919.4965	0.22	0.44
9	0.0016	0.5270	0.3718	5.08x10 ⁻⁵	137515.0209	20.6616	-293.1001	-596707.0878	0.24	0.49
10	0.0008	0.8165	0.2811	5.08x10 ⁻⁵	183099.0908	26.8000	-438.6867	-780230.9540	0.19	0.39

Table 6-3: Combined uncertainty and expanded uncertainty values using bottle with four holes in pouring cap next 10 participants

Participant	Standard uncertainties				Sensitivity coefficients				Combined standard uncertainty	Expanded uncertainty
	$u(F_1)$ (N)	$u(p_D)$	$u(p_{d1})$	$u(D)$ (m)	dP_l/dF_1	dP_l/dp_D	dP_l/dp_{d1}	dP_l/dD		
11	0.0028	0.6325	0.7177	5.08x10 ⁻⁵	96545.6296	18.2262	-216.6404	-512871.2250	0.31	0.62
12	0.0010	0.0000	0.3331	5.08x10 ⁻⁵	100216.7612	6.7006	-81.1452	-198547.4703	0.10	0.21
13	0.0020	0.0000	0.4181	5.08x10 ⁻⁵	96064.7169	13.4076	-158.9684	-344497.4256	0.21	0.42
14	0.0027	0.3162	0.2108	5.08x10 ⁻⁵	145937.2968	15.1033	-220.7158	-367021.2335	0.40	0.80
15	0.0012	0.0000	0.5077	5.08x10 ⁻⁵	177268.4248	58.7138	-945.6557	-1383898.3498	0.53	1.05
16	0.0013	0.4216	0.2582	5.08x10 ⁻⁵	82334.9040	9.6504	-105.9291	-234861.5633	0.11	0.22
17	0.0017	0.0000	0.4181	5.08x10 ⁻⁵	154082.2236	15.8199	-237.5515	-385172.0252	0.28	0.55
18	0.0007	0.3162	0.3375	5.08x10 ⁻⁵	97434.3731	14.5920	-174.2404	-350665.0664	0.09	0.18
19	0.0013	0.0000	0.5164	5.08x10 ⁻⁵	155385.9002	38.1134	-574.7265	-937830.7566	0.36	0.72
20	0.0027	0.5164	0.3996	5.08x10 ⁻⁵	74207.8148	8.7867	-91.5643	-218665.1510	0.21	0.41

Table 6-4: Combined uncertainty and expanded uncertainty values using syringe for first 10 participants

Participant	Standard uncertainties				Sensitivity coefficients						Combined standard uncertainty	Expanded uncertainty
	$u(F_1)$ (N)	$u(p_D)$	$u(p_{d1})$	$u(D)$ (m)	dP/dF_1	dP/dp_D	dP/dp_{d1}	dP/dD	u_c (kPa)	U (kPa)		
1	0.0025	0.4830	0.4216	5.08x10 ⁻⁵	552832.8130	144.2509	-1834.8802	-6349461.0529	1.63	3.27		
2	0.0031	0.0000	0.3162	5.08x10 ⁻⁵	837894.3403	356.6099	-5584.4486	-9864779.1289	3.17	6.34		
3	0.0013	0.3162	0.5164	5.08x10 ⁻⁵	974618.7600	275.0670	-4645.6678	-8037987.2254	2.75	5.50		
4	0.0045	0.0000	0.0000	5.08x10 ⁻⁵	771545.6657	224.1658	-3368.5452	-6456494.6514	3.45	6.91		
5	0.0061	0.3162	0.4216	5.08x10 ⁻⁵	678609.9712	275.8712	-3887.8438	-8015757.5034	4.45	8.90		
6	0.0027	0.5164	0.5164	5.08x10 ⁻⁵	1028368.072	298.4879	-5178.3720	-8154916.5749	3.89	7.78		
7	0.0019	0.3162	0.0000	5.08x10 ⁻⁵	662103.6318	315.5692	-4392.8854	-8874975.6062	1.34	2.68		
8	0.0019	0.4830	0.5164	5.08x10 ⁻⁵	879085.0899	384.3692	-6165.3301	-10347943.1595	3.65	7.29		
9	0.0018	0.4216	0.4216	5.08x10 ⁻⁵	821171.1528	255.6791	-3963.7316	-7433023.4518	2.26	4.52		
10	0.0031	0.5164	0.4830	5.08x10 ⁻⁵	675596.1006	215.7224	-3032.9603	-6331760.3599	2.57	5.13		

Table 6-5: Combined uncertainty and expanded uncertainty values using syringe for next 10 participants

Participant	Standard uncertainties				Sensitivity coefficients				Combined standard uncertainty	Expanded uncertainty
	$u(F_1)$ (N)	$u(p_D)$	$u(p_{AI})$	$u(D)$ (m)	dP_I/dF_1	dP_I/dp_D	dP_I/dp_{AI}	dP_I/dD		
11	0.0020	0.4216	0.4830	5.08×10^{-5}	727302.2182	183.8027	-2681.6475	-5181591.9094	1.98	3.97
12	0.0050	0.0000	0.3162	5.08×10^{-5}	516334.1073	165.4180	-2033.4829	-4961512.9051	2.68	5.37
13	0.0018	1.2517	0.4830	5.08×10^{-5}	576515.9688	258.3102	-3355.3633	-6726717.8530	1.98	3.95
14	0.0017	0.4216	0.5164	5.08×10^{-5}	694564.4316	266.1098	-3794.1055	-6407368.4115	2.30	4.60
15	0.0016	0.5164	0.5270	5.08×10^{-5}	711628.3742	419.7858	-6058.2422	-9885755.7594	3.45	6.89
16	0.0048	0.0000	0.3162	5.08×10^{-5}	688898.4842	458.3904	-6508.8662	-11160561.1468	3.93	7.86
17	0.0016	0.6992	0.4830	5.08×10^{-5}	586524.2092	256.2075	-3356.8120	-6312281.1413	1.91	3.81
18	0.0014	0.9189	0.4216	5.08×10^{-5}	880693.9318	416.1055	-6680.4882	-10105172.7601	3.12	6.25
19	0.0021	0.0000	0.0000	5.08×10^{-5}	710888.5619	771.9970	-11135.4724	-19035981.5393	1.80	3.59
20	0.0018	0.3162	0.3162	5.08×10^{-5}	578397.1981	322.9309	-4201.6029	-8031451.8682	1.74	3.47

Table 6-6: Combined uncertainty and expanded uncertainty values using pressurized device for first 10 participants

Participant	Standard uncertainties				Sensitivity coefficients				Combined standard uncertainty	Expanded uncertainty
	$u(F_1)$ (N)	$u(p_D)$	$u(p_{AI})$	$u(D)$ (m)	dP_1/dF_1	dP_1/dp_D	dP_1/dp_{AI}	dP_1/dD		
1	0.0010	0.4216	0.5270	5.08x10-5	74046.8887	34.9719	-363.9654	-1536952.5188	0.22	0.44
2	0.0008	0.4830	0.5164	5.08x10-5	77893.4451	66.2475	-707.2891	-1370317.7560	0.38	0.76
3	0.0019	0.8756	0.4830	5.08x10-5	88362.5913	74.9222	-851.9650	-1354917.4788	0.46	0.91
4	0.0016	0.4216	0.5164	5.08x10-5	82590.0586	89.0020	-978.4555	-1591561.4283	0.53	1.06
5	0.0046	0.4216	0.0000	5.08x10-5	86390.8720	132.5877	-1490.7825	-2471251.5304	0.42	0.83
6	0.0021	0.0000	0.4830	5.08x10-5	79634.1597	60.0585	-648.3378	-1098251.5023	0.36	0.72
7	0.0052	0.4216	0.4830	5.08x10-5	76595.6522	119.1635	-1261.6030	-2137091.7040	0.74	1.48
8	0.0013	0.3162	0.4216	5.08x10-5	66491.0374	59.3107	-585.0489	-1115302.4205	0.27	0.53
9	0.0012	1.5811	0.5270	5.08x10-5	100759.7933	98.8895	-1200.8008	-1959450.1867	0.67	1.34
10	0.0008	0.5164	0.5164	5.08x10-5	74966.9215	104.1759	-1091.1370	-1955726.3603	0.58	1.16

Table 6-7: Combined uncertainty and expanded uncertainty values using pressurized device for next 10 participants

Participant	Standard uncertainties				Sensitivity coefficients				Combined standard uncertainty	Expanded uncertainty
	$u(F_{11})$ (N)	$u(p_D)$	$u(p_{d1})$	$u(D)$ (m)	dP_{11}/dF_{11}	dP_{11}/dp_D	dP_{11}/dp_{d1}	dP_{11}/dD		
11	0.0019	0.4216	0.0000	5.08×10^{-5}	92348.8347	115.5850	-1343.6755	-2227394.1893	0.22	0.43
12	0.0011	0.5270	0.5164	5.08×10^{-5}	87462.8095	72.4168	-819.2719	-1341120.5760	0.44	0.88
13	0.0015	0.4216	0.4830	5.08×10^{-5}	107703.7919	126.8540	-1592.5639	-2202727.7789	0.80	1.59
14	0.0014	0.5164	0.5164	5.08×10^{-5}	77535.3148	87.3021	-929.9330	-1522269.1832	0.50	1.00
15	0.0014	0.5164	0.4216	5.08×10^{-5}	88517.4418	150.4013	-1711.7618	-2465135.5540	0.75	1.50
16	0.0014	0.3162	0.5676	5.08×10^{-5}	70209.6682	69.5423	-704.8957	-1099117.3709	0.42	0.83
17	0.0017	0.4830	0.0000	5.08×10^{-5}	84091.4077	96.2464	-1067.6709	-1603939.9245	0.17	0.35
18	0.0014	0.0000	0.5164	5.08×10^{-5}	91706.6042	108.7657	-1259.9971	-1853704.7742	0.67	1.34
19	0.0044	0.3162	0.5164	5.08×10^{-5}	97349.6623	147.4302	-1759.6689	-2406509.4709	1.01	2.03
20	0.0010	0.6992	0.5164	5.08×10^{-5}	84114.0165	51.7901	-574.5897	-881053.3638	0.31	0.63

7. RESULTS AND DISCUSSION

7.1 Pressure obtained at wound area (target area)

7.1.1 Mean pressure obtained in each trial

Figure 7.1 plots the mean pressure obtained for all 20 participants using the three irrigation devices. The error bars represent the expanded uncertainty associated with each measurement.

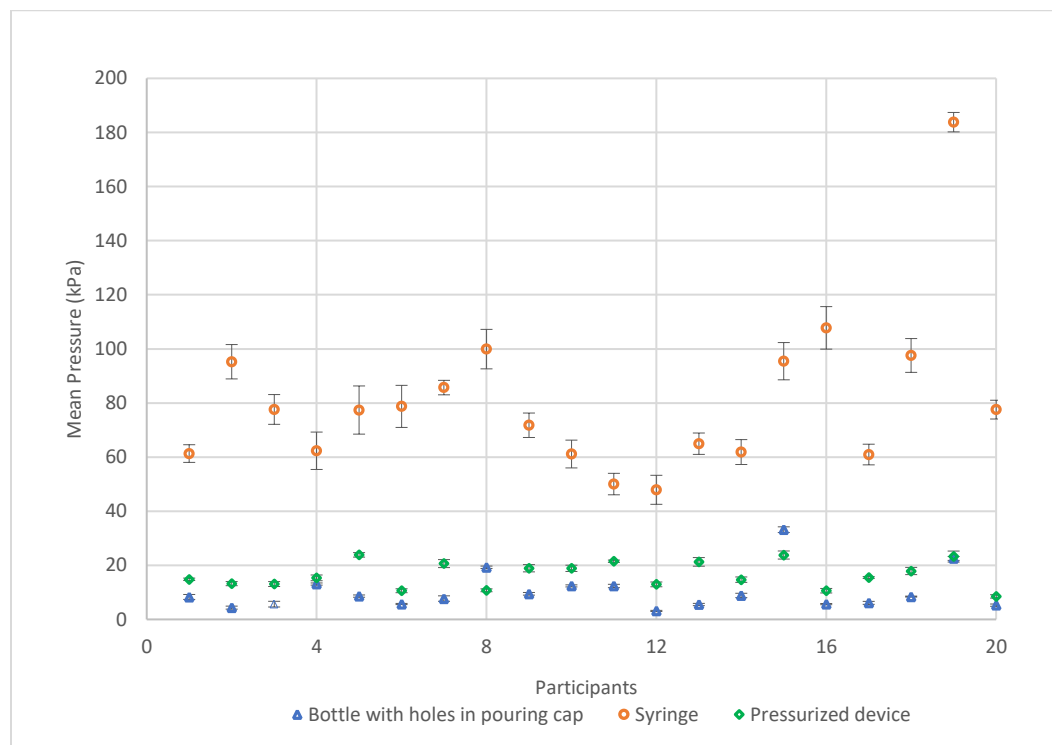


Figure 7-1 Mean pressure for all participants with expanded uncertainty associated with each trial

The variation between the maximum and minimum mean pressure between all participants was also calculated. This identifies the level of variation between trained medical professionals using the same device in a single setting.

- Bottle with four holes in the pouring cap: 30.04 kPa
- Syringe: 135.9 kPa
- Pressurized device: 15.35 kPa

The mean pressures obtained for all participants using the three irrigation devices are shown in Table 7.1, along with the uncertainty values.

Table 7-1: Mean pressure for all participants with expanded uncertainty estimation

Participant	Bottle with four holes in pouring cap		Syringe		Pressurized device	
	Mean pressure (kPa)	Expanded uncertainty (kPa)	Mean pressure (kPa)	Expanded uncertainty (U)	Mean pressure (kPa)	Expanded uncertainty (kPa)
1	8.31	0.92	61.3	3.3	14.83	0.44
2	4.35	0.56	95.25	6.34	13.23	0.76
3	5.65	1.05	77.61	5.50	13.08	0.91
4	13.08	0.41	62.34	6.91	15.37	1.06
5	8.62	0.42	77.40	8.90	23.86	0.83
6	5.70	0.21	78.74	7.78	10.60	0.72
7	7.71	1.00	85.70	2.68	20.64	1.48
8	19.28	0.44	99.92	7.29	10.77	0.53
9	9.47	0.49	71.77	4.52	18.92	1.34
10	12.40	0.39	61.14	5.13	18.88	1.16
11	12.35	0.62	50.03	3.97	21.51	0.43
12	3.14	0.21	47.91	5.37	12.95	0.88
13	5.51	0.42	64.95	3.95	21.27	1.59
14	8.86	0.80	61.87	4.60	14.70	1.00
15	33.18	1.05	95.46	6.89	23.80	1.50
16	5.66	0.22	107.77	7.86	10.61	0.83
17	6.12	0.55	60.95	3.81	15.49	0.35
18	8.44	0.18	97.58	6.25	17.90	1.34
19	22.54	0.72	183.81	3.59	23.24	2.03
20	5.28	0.41	77.55	3.47	8.51	0.63

7.1.2 Mean of mean pressures for each irrigation device

Figure 7.2 plots the mean of all the mean pressures obtained using each irrigation device. It was calculated by taking the mean of the mean pressure for each participant using the selected irrigation device. The error bars represent the mean of the expanded uncertainties.

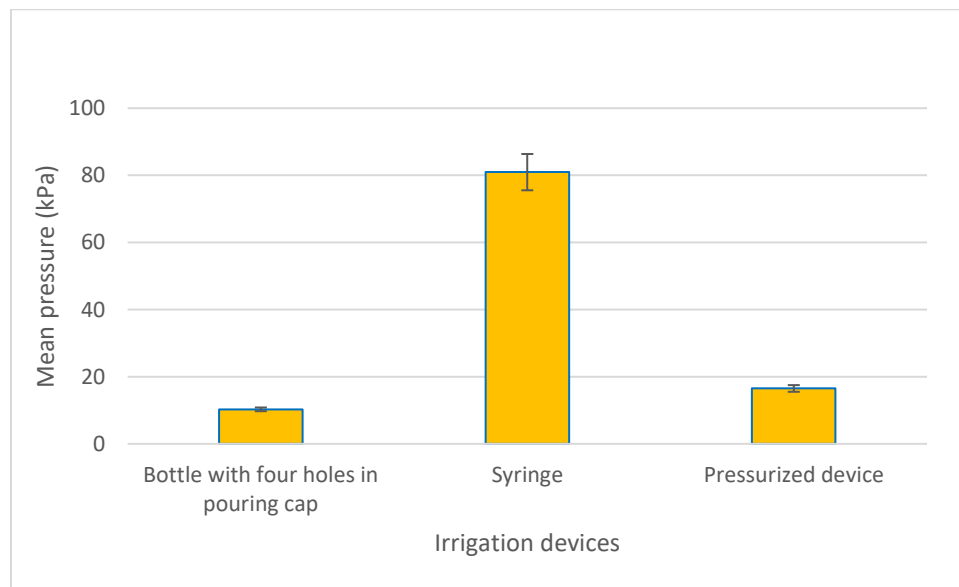


Figure 7-2 Mean pressure of all participants with mean expanded uncertainty for the three irrigation devices

From Figure 7.2, the mean pressure of all the participants using an irrigation device are:

- Bottle with four holes in the pouring cap: 10.28 kPa
- Syringe: 80.95 kPa
- Pressurized device: 15.50 kPa

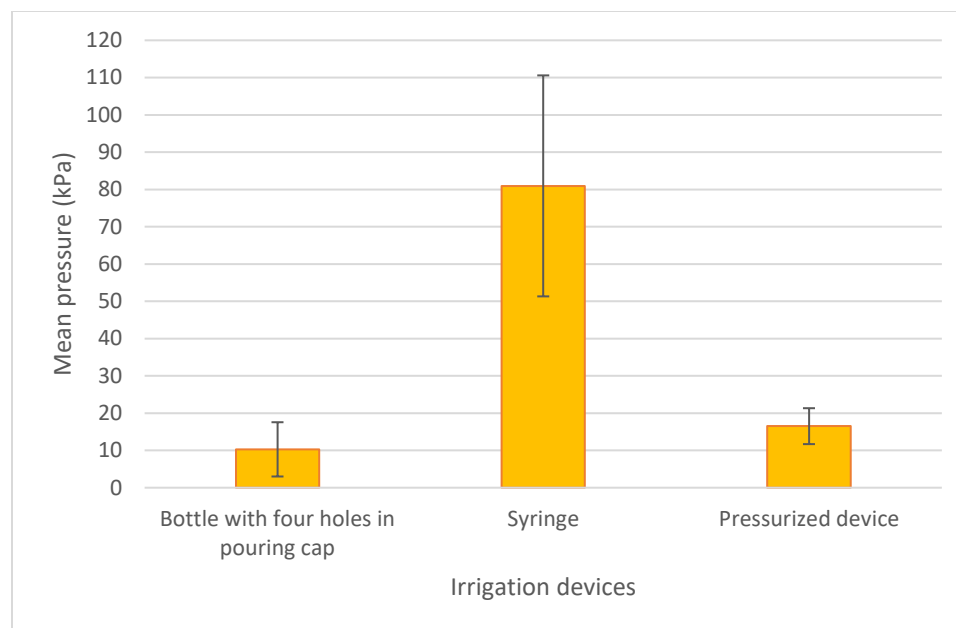


Figure 7-3 Standard deviation of mean pressures for each irrigation device

Figure 7.3 displays the standard deviation of all the mean pressures obtained using each irrigation device. The error bars represent the standard deviation of the mean pressure of all participants. The standard deviation of mean pressure of all the participants using an irrigation device were:

- Bottle with four holes in the pouring cap: 7.27 kPa
- Syringe: 29.64 kPa
- Pressurized device: 4.82 kPa

7.1.3 Minimum, maximum, and mean pressures calculated for all trials

Figures 7.4-7.6 show the mean, maximum, and minimum pressures obtained by the participants using the three irrigation devices. The upper and lower endpoints of the error bars represent the maximum and minimum calculated pressure for the selected participant over all intervals in the trial. For the bottle and syringe, there were multiple intervals so

these maximum and minimum values were selected from all intervals in a single trial. For the pressurized device these values were obtained from the sole interval in the trial.

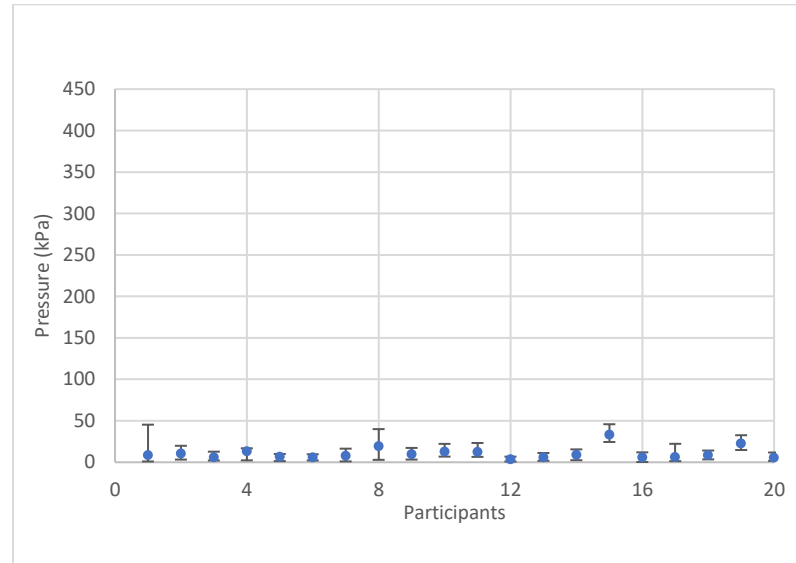


Figure 7-4 Mean, maximum, and minimum pressures for all participants using the bottle with four holes in the pouring cap

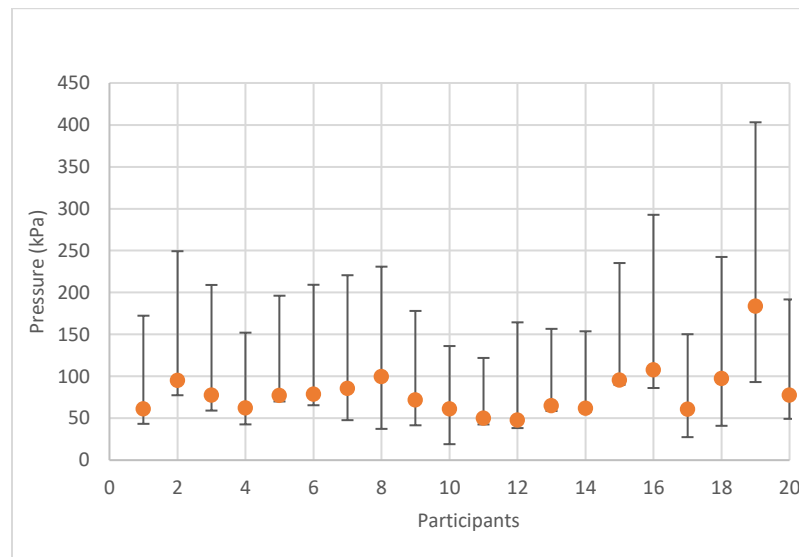


Figure 7-5 Mean, maximum, and minimum pressures for all participants using the 60 ml syringe

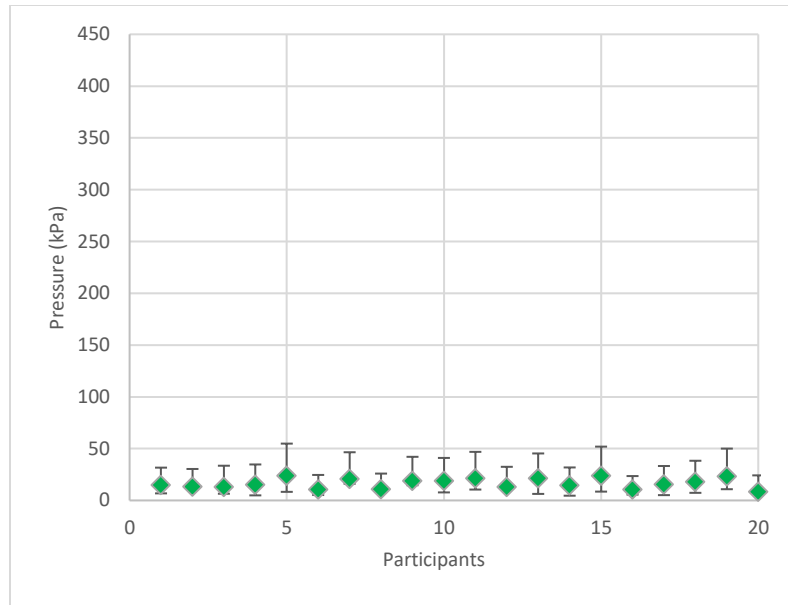


Figure 7-6 Mean, maximum, and minimum pressures for all participants using the pressurized device

7.2 Force obtained at wound area (target area)

7.2.1 Mean force obtained in each trial

Figure 7.7 displays the mean force obtained for all 20 participants using the three irrigation devices.

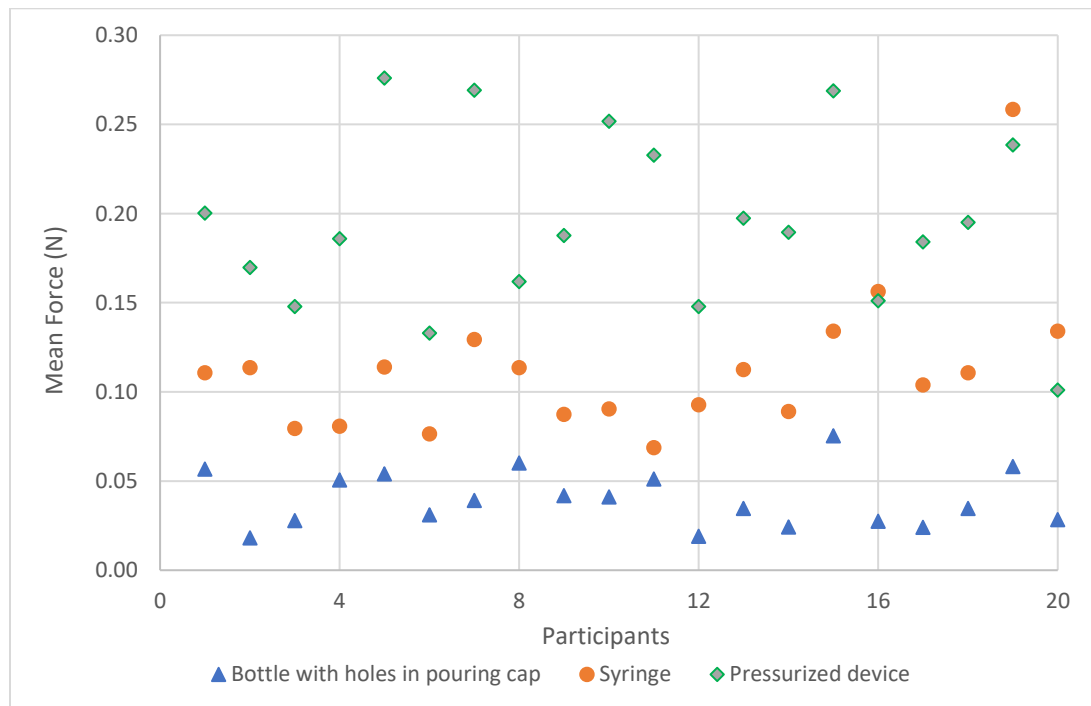


Figure 7-7 Mean force for all trials using the three irrigation devices

7.2.2 Mean of mean force for each irrigation device

Figure 7.8 displays the mean of all the mean forces obtained using each irrigation device. The force was determined by calculating the mean of the mean forces for each participant using the irrigation device.

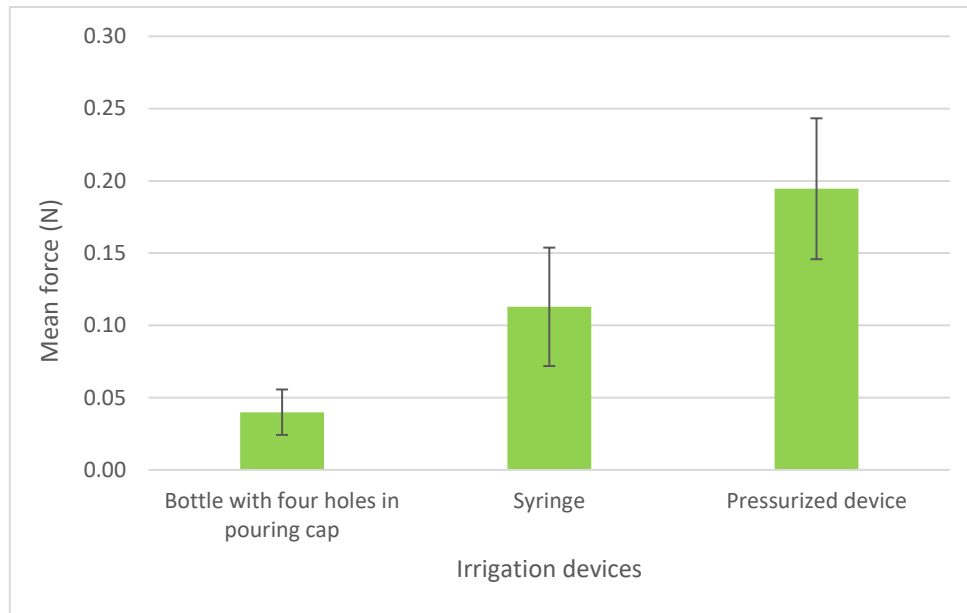


Figure 7-8 Mean force for all trials using the three irrigation devices

The error bars represent the standard deviation of the mean force of all participants.

The standard deviations of mean force of all the participants using an irrigation device are:

- Bottle with four holes in the pouring cap: 0.016 N
- Syringe: 0.04 N
- Pressurized device: 0.048 N

7.3 Time taken for fluid irrigation

7.3.1 Duration of each trial

Figure 7.9 displays the duration of each trial for all 20 participants using the three irrigation devices. The trial started when the fluid impacted the target area and ended when the full 500 ml of irrigation fluid was dispensed.

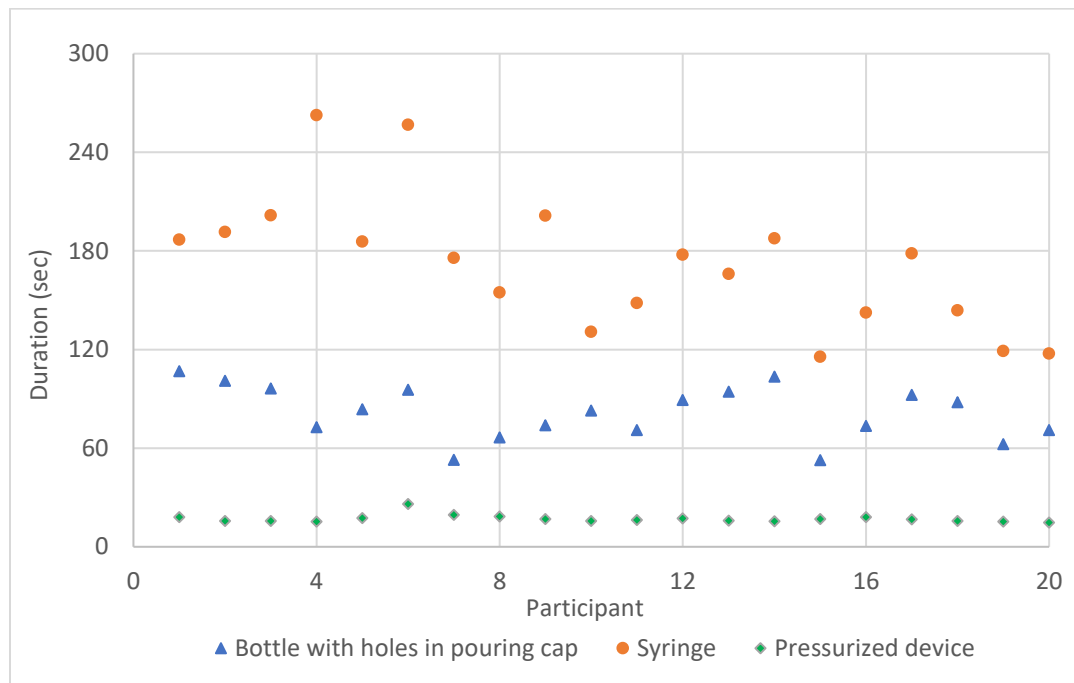


Figure 7-9 Duration of each trial for all participants using the three irrigation devices

The mean duration of a trial (i.e., the time taken for a participant to dispense 500 ml using an irrigation device) were:

- Bottle with four holes in the pouring cap: 81 secs
- Syringe: 172 secs
- Pressurized device: 17 secs

7.3.2 Standard deviation of duration of each trial

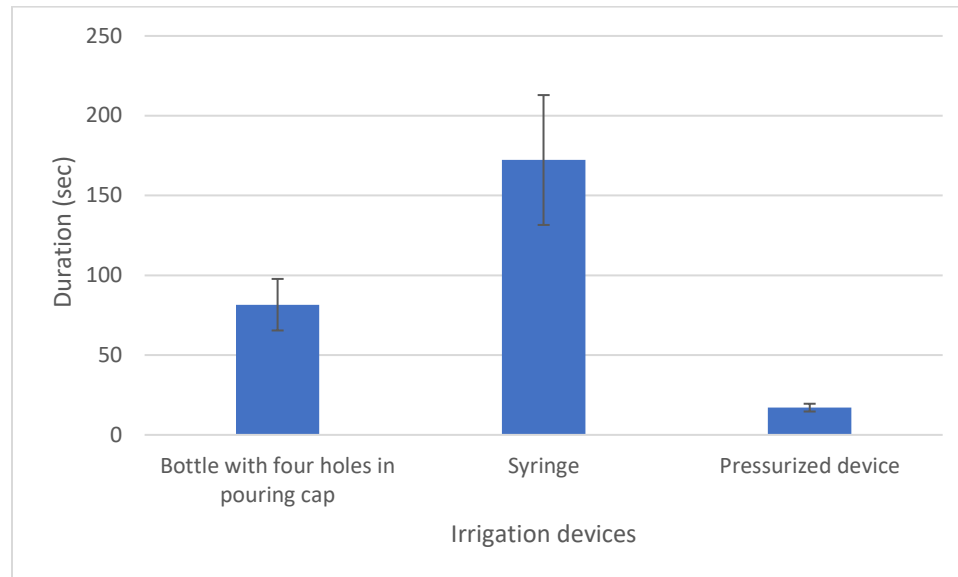


Figure 7-10 Standard deviation of mean trial duration of all participants

Figure 7.10 displays the standard deviations for the duration of each trial from all 20 participants using the three irrigation devices. The standard deviations of the mean trial duration of all the participants using an irrigation device are:

- Bottle with four holes in the pouring cap: 16 secs
- Syringe: 40 secs
- Pressurized device: 2 secs

8. CONCLUSION

The purpose of this study was to serve the medical community by studying the pressure imposed on wounds by three common irrigation devices, reporting the experimental techniques, and evaluating the measurement uncertainty. To collect data for the study, 20 doctors and nurses conducted wound irrigation trials using: 1) a bottle with four holes in the pouring cap; 2) a syringe; and 3) a pressurized irrigation device. The motivation for the study was based on a literature review. The current literature does not contain a standard pressure measurement method for wound irrigation. Further, there is no consensus on what pressure is required for proper irrigation. It is anticipated that this study will help to standardize irrigation pressure measurement within the community.

The study results are summarized here. From Figure 7.2 it can be observed that the mean pressure obtained from all participants is the highest for the 60 ml syringe. The bottle with four holes in the pouring cap had the lowest mean pressure. However, the pressure uncertainty for the syringe was also the highest. Further, the standard deviation of mean pressures from all participants (as shown in Figure 7.3) was the highest for the syringe. The pressurized irrigation device had the lowest standard deviation of mean pressures from all participants.

Observing Figure 7.7, the mean duration of a single trial (500 ml dispensation of fluid) was the highest for the 60 ml syringe. The pressurized irrigation device required the lowest time. Finally, from Figure 7.8, it can be observed that the standard deviation of trial durations is maximum for the 60 ml syringe and minimum for the pressurized irrigation device.

An analytical check was performed to verify the wound pressure value obtained due to the pressurized irrigation device for an example trial (participant 13). This was done by using mass flow rate and fluid velocity to theoretically calculate force at the wound area.

$$\text{Area of fluid streams, } A = 9.28 \times 10^{-6} \text{ m}^2$$

$$\text{Volume of fluid emptied, } V = 500 \text{ ml} = 500 \times 10^{-6} \text{ m}^3$$

$$\text{Time required to empty 500 ml of water, } t = 16 \text{ sec}$$

$$\therefore \text{Flow rate, } Q = \frac{V}{t} = \frac{500 \times 10^{-6}}{16}$$

$$Q = 3.125 \times 10^{-5} \text{ m}^3/\text{s}$$

$$\text{Fluid velocity before impact, } v_{in} = \frac{Q}{A} = \frac{3.125 \times 10^{-5}}{9.28 \times 10^{-6}}$$

$$v_{in} = 3.367 \text{ m/s}$$

By Newton's second law, $F = \text{mass} \times \text{acceleration}$

$= \text{mass flow rate} \times \text{change in velocity}$

$$= \dot{m}(v_{in} - v_{out})$$

$$\therefore F = \dot{m}(v_{in}) \quad [\because \text{fluid velocity after impact, } v_{out} = 0]$$

$$= \partial Q v_{in}$$

$$= \partial (v_{in} A) v_{in}$$

$$\therefore F = \partial A v_{in}^2$$

Substituting known values,

$$F = 1000 \times (9.28 \times 10^{-6}) \times (3.367)^2 \quad [\because \text{Density of water} = 1000 \text{ kg/m}^3]$$

$$\therefore F = 0.105 \text{ N}$$

$$\therefore \text{Pressure at impact, } P = \frac{F}{A} = \frac{0.105}{9.28 \times 10^{-6}}$$

$$P = 11.34 \text{ kPa}$$

$$\therefore P = 1.6 \text{ psi}$$

The pressurized irrigation device experimental value for participant 13 was 21.27 kPa or 3.08 psi.

REFERENCES

- [1] Skinner, H. G., Blanchard, J., & Elixhauser, A. (2014). Trends in emergency department visits, 2006–2011. *Statistical Brief*, 179.
- [2] Nicks, B. A., Ayello, E. A., Woo, K., Nitzki-George, D., & Sibbald, R. G. (2010). Acute wound management: revisiting the approach to assessment, irrigation, and closure considerations. *International journal of emergency medicine*, 3(4), 399-407.
- [3] Singer, A. J., & Dagum, A. B. (2008). Current management of acute cutaneous wounds. *New England Journal of Medicine*, 359(10), 1037-1046.
- [4] Singer, A. J., Hollander, J. E., Subramanian, S., Malhotra, A. K., & Villez, P. A. (1994). Pressure dynamics of various irrigation techniques commonly used in the emergency department. *Annals of emergency medicine*, 24(1), 36-40.
- [5] Atiyeh, B. S., Dibo, S. A., & Hayek, S. N. (2009). Wound cleansing, topical antiseptics and wound healing. *International wound journal*, 6(6), 420-430.
- [6] Ennis, W. J., Valdes, W., Salzman, S., Fishman, D., & Meneses, P. (2004). Trauma and wound care. *Chronic Wound Care. A Problem-Based Learning Approach*, 291-307.
- [7] Wu, F., & Winters, M. E. (2017). *Emergency Medicine, An Issue of Physician Assistant Clinics, E-Book* (Vol. 2). Elsevier Health Sciences.
- [8] Mitra, E. S., Singer, A. J., & Bluestein, D. (2003). Hol-7. lander JE. *Simulated wound irrigation impact pressures. Israeli J Emerg Med*, 3, 9-16.
- [9] Wedmore, L. I. S., Godwin, S. A., & Howell, J. M. (2005). Wound care: modern evidence in the treatment of man's age-old injuries. *Emergency Medicine Practice+ Em Practice Guidelines Update*, 7(3), 1-23.
- [10] Pronchik, D., Barber, C., & Rittenhouse, S. (1999). Low-versus high-pressure irrigation techniques in Staphylococcus aureus-inoculated wounds. *The American journal of emergency medicine*, 17(2), 121-124.
- [11] Elizabeth Palermo, “What is Stereolithography?” Live Science September 19, 2013. <<https://www.livescience.com/39810-fused-deposition-modeling.html>>
- [12] Elizabeth Palermo, “Fused Deposition Modeling: Most Common 3D Printing Method” Live Science September 19, 2013. <https://www.livescience.com/39810-fused-deposition-modeling.html>
- [13] Chen, K. Y., Janz, K. F., Zhu, W., & Brychta, R. J. (2012). Re-defining the roles of sensors in objective physical activity monitoring. *Medicine and science in sports and exercise*, 44(1 Suppl 1), S13.

- [14] “*MiniDyn Multicomponent Dynamometer up to 250 N*”, Kistler Group 2018.
- [15] “*Kistler 9256C1 Multicomponent Dynamometer Triaxial Force Sensor Special Hole Pattern*”, Hofstra Group. <<https://www.hofstragroup.com/product/kistler-9256c1-multicomponent-dynamometer-triaxial-force-sensor-special-hole-pattern/>>
- [16] “*Charge Amplifier Multichannel Laboratory Charge Amplifier*”, Kistler Group 2018.
- [17] “*What is Data Acquisition?*”, National Instruments 2018. <<http://www.ni.com/data-acquisition/what-is/>>
- [18] “*DT9837 Series User’s Manual*”, Data Translation- A Measurement Computing Company.
- [19] “*Canon EOS 1200D DSLR Camera*”, Canon 2018. <https://www.canon.co.uk/for_home/product_finder/cameras/digital_slr/eos_1200d/>
- [20] Vijayaraghavan, G., Brown, M., & Barnes, M. (2004). *Practical grounding, bonding, shielding and surge protection*. Elsevier.
- [21] Smith, S. (2013). *Digital signal processing: a practical guide for engineers and scientists*. Elsevier.
- [22] “*Butterworth filter design*”, The MathWorks, Inc 1994-2018. <<https://www.mathworks.com/help/signal/ref/butter.html>>
- [23] Smith, J. O. (2007). *Introduction to digital filters: with audio applications* (Vol. 2). Julius Smith.
- [24] “*Industrial measurements*”, Control Global 2004 - 2013. <<https://www.controlglobal.com/articles/2011/industrialmeasurements1104/>>
- [25] Kleckers, T. (2013). A1. 1-Electrical Strain Gauges, Piezoelectric Sensors or Fiber Bragg Sensors for Force Measurement: Prospects and Potentials. *Proceedings SENSOR 2013*, 23-27.
- [26] Mack, O. (2001, September). New procedures to characterize drift and non-linear effects of piezoelectric force sensors. In *Proceedings of the IMEKO TC3 Conference. Istanbul, Turkey*.
- [27] Klein, C. A., Olson, K. W., & Pugh, D. R. (1983). Use of force and attitude sensors for locomotion of a legged vehicle over irregular terrain. *The International Journal of Robotics Research*, 2(2), 3-17.

- [28] Dong, G., & Xie, M. (2005). Color clustering and learning for image segmentation based on neural networks. *IEEE transactions on neural networks*, 16(4), 925-936.
- [29] Senthilkumaran, N., & Rajesh, R. (2009). Edge detection techniques for image segmentation—a survey of soft computing approaches. *International journal of recent trends in engineering*, 1(2), 250-254.
- [30] Efford, N. (2000). *Digital image processing: a practical introduction using java (with CD-ROM)*. Addison-Wesley Longman Publishing Co., Inc..
- [31] Canny, J. (1987). A computational approach to edge detection. In *Readings in Computer Vision* (pp. 184-203).
- [32] Heath, M., Sarkar, S., Sanocki, T., & Bowyer, K. (1998). Comparison of edge detectors: a methodology and initial study. *Computer vision and image understanding*, 69(1), 38-54.
- [33] Rani, S., Bansal, D., & Kaur, B. (2014). Detection of edges using mathematical morphological operators. *open transactions on information processing*, 1(1), 17-26.
- [34] Hanumantharaju, M. C., Ravishankar, M., & Rameshbabu, D. R. (2013). Design of novel algorithm and architecture for Gaussian based color image enhancement system for real time applications. In *Advances in Computing, Communication, and Control* (pp. 595-608). Springer, Berlin, Heidelberg.
- [35] Juneja, M., & Sandhu, P. S. (2009). Performance evaluation of edge detection techniques for images in spatial domain. *international journal of computer theory and Engineering*, 1(5), 614.
- [36] Kaur, P., & Maini, R. (2013). Performance Evaluation of various thresholding methods using canny edge detector. *International Journal of Computer Applications*, 71(9).
- [37] Fang, M., Yue, G., & Yu, Q. (2009, August). The study on an application of otsu method in canny operator. In *International Symposium on Information Processing (ISIP)* (pp. 109-112).
- [38] Henstock, P. V., & Chelberg, D. M. (1996). Automatic gradient threshold determination for edge detection. *IEEE transactions on image processing*, 5(5), 784-787.
- [39] Level Otsu, N. (1979). A threshold selection method from gray-level histogram. *IEEE Trans. Syst. Man Cybern*, 9(1), 62-66.
- [40] “G104 - Guide for Estimation of Measurement Uncertainty In Testing”, American Association for Laboratory Accreditation, 2014
- [41] “ABS Digimatic Caliper CD-AX/APX Series”, Mitutoyo Corporation